Electronic Supplementary Information

Carbazole sulfonamide-based macrocyclic receptors capable of selective complexation of fluoride ion

Na Luo,[a] Junhong Li,[a] Tao Sun,[b] Suran Wan,[a] Peijia Li,[a] Nan Wu,[a] Ya Yan,[a] Xiaoping Bao*,[a]

[a]*State Key Laboratory Breeding Base of Green Pesticide and Agricultural Bioengineering, Key Laboratory of Green Pesticide and Agricultural Bioengineering, Ministry of Education, Center for Research and Development of Fine Chemicals, Guizhou University, Guiyang 550025, China.*

**Corresponding author: baoxp_1980@aliyun.com*

[b]*College of Chemistry and Chemical Engineering, Guizhou Key Laboratory of High Performance Computational Chemistry, Guizhou University, Guiyang 550025, China.*

Table of Contents

1. Crystal data

Table S1. Crystal data for macrocycle **1**, its fluoride complex ([**1**]$_2$·TBAF), and macrocycle **2**.

	macrocycle **1**	[**1**]$_2$·TBAF	macrocycle **2**
CCDC number	**1976672**	**1976667**	**2021529**
Empirical formula	$C_{28}H_{33}N_3O_4S_2$	$C_{72}H_{102}FN_7O_8S_4$	$C_{27}H_{32}N_4O_4S_2$
Formula weight	539.69	1340.84	540.68
Temperature/K	150.03	273.15	273.00
Wavelength/Å	1.54178	1.54178	0.71073
Crystal system	orthorhombic	orthorhombic	monoclinic
Space group	$P2_12_12_1$	$P2_12_12_1$	$P2_1/n$
a/Å	18.5696(4)	16.4040(17)	30.948(4)
b/Å	26.4247(6)	16.5999(19)	6.6912(8)
c/Å	6.5248(1)	29.9980(4)	30.949(4)
α/°	90	90	90
β/°	90	90	119.496(4)
γ/°	90	90	90
V/Å^3	3201.69(11)	8168.7(16)	5578.3(12)
Z	4	4	8
D_{calc}/g cm^{-3}	1.120	1.090	1.288
Absorption coefficient/mm^{-1}	1.776	1.496	0.230
F(000)	1144.0	2880.0	2288.0
Crystal size/mm^3	0.24 × 0.22 × 0.19	0.38 × 0.31 × 0.12	0.15 × 0.15 × 0.12
Radiation, λ/Å	CuKα (λ = 1.54178)	CuKα (λ = 1.54178)	MoKα (λ = 0.71073)
2Θ range /°	5.816 to 144.236	5.892 to 134.036	1.512 to 56.67
Index ranges	$-22 \le h \le 22$, $-32 \le k \le 32$, $-7 \le l \le 6$	$-19 \le h \le 19$, $-19 \le k \le 19$, $-35 \le l \le 35$	$-41 \le h \le 41$, $-8 \le k \le 8$, $-41 \le l \le 41$
Reflections collected	21398	100660	172216
Independent reflections	6171 [R_{int} = 0.0355, R_{sigma} = 0.0297]	14480 [R_{int} = 0.1695, R_{sigma} = 0.1056]	13837 [R_{int} = 0.0934, R_{sigma} = 0.0397]
Data/restraints/parameters	6171/135/371	14480/134/906	13837/156/731
Goodness-of-fit on F^2	1.081	1.018	1.069
Final R indexes [$I \ge 2\sigma(I)$]	R_1 = 0.0834, wR_2 = 0.2191	R_1 = 0.0803, wR_2 = 0.2048	R_1 = 0.0568, wR_2 = 0.1334
Final R indexes [all data]	R_1 = 0.0879, wR_2 = 0.2240	R_1 = 0.1309, wR_2 = 0.2396	R_1 = 0.0771, wR_2 = 0.1452
Largest diff. peak/hole/e Å^{-3}	0.61/−0.36	0.30/−0.55	0.61/−0.35

2. ^{1}H NMR titration studies

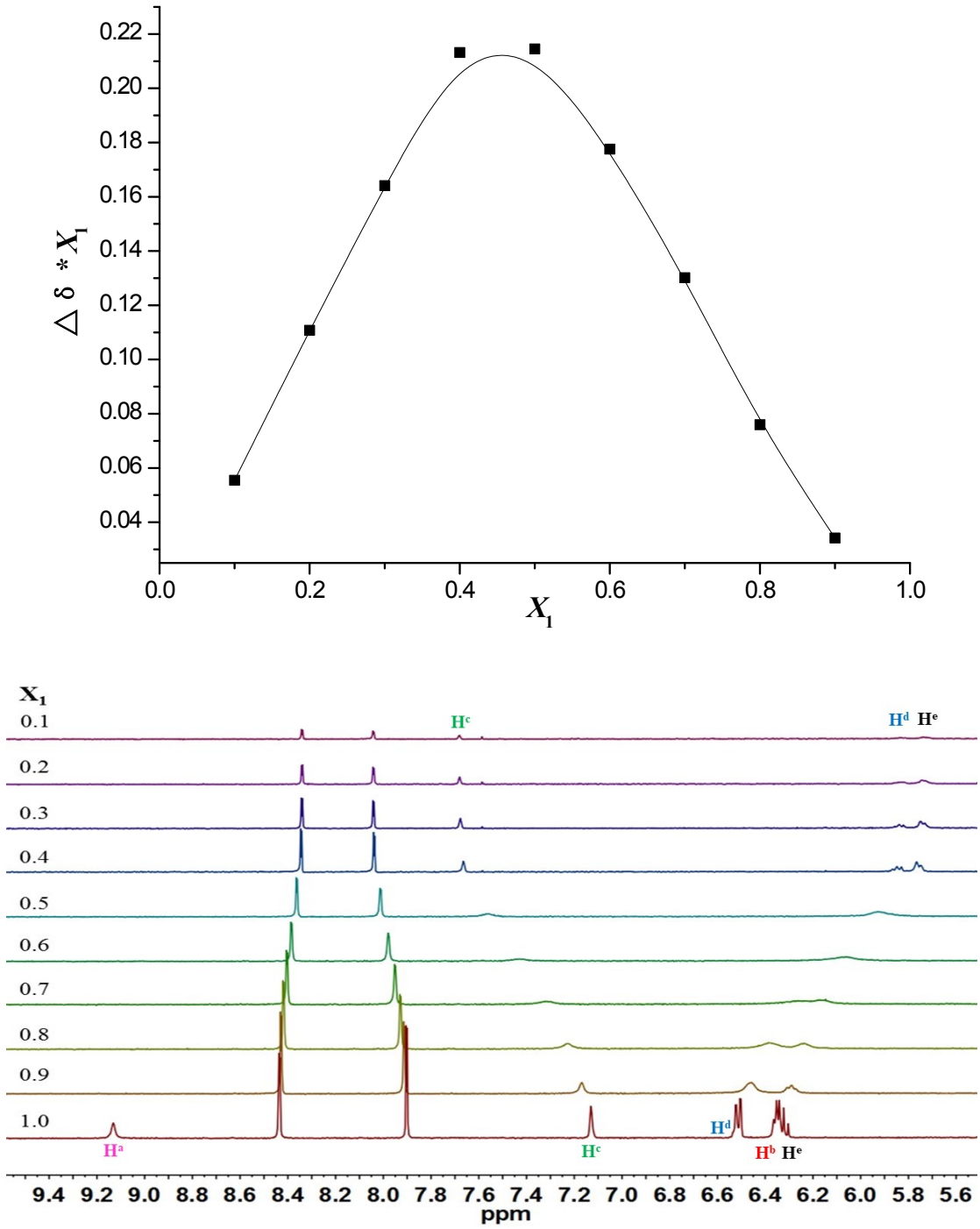

Figure S1. Job's plot of macrocycle **1** with TBAF (monitoring the chemical shift of the proton H^c) in CD_3CN at 298 K with a total concentration of 1.0 mM (top) and the corresponding ^{1}H NMR spectra (bottom).

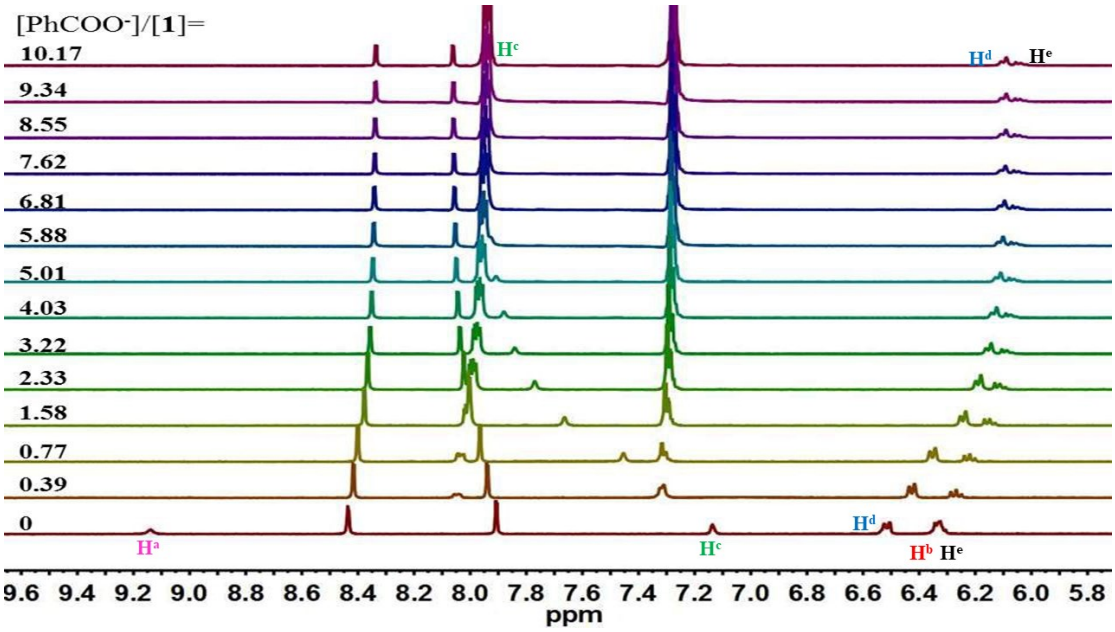

Figure S2. Stack plot of ^{1}H NMR titration of macrocycle **1** (1.6 mM) with TBAPhCOO in CD_3CN at 298 K.

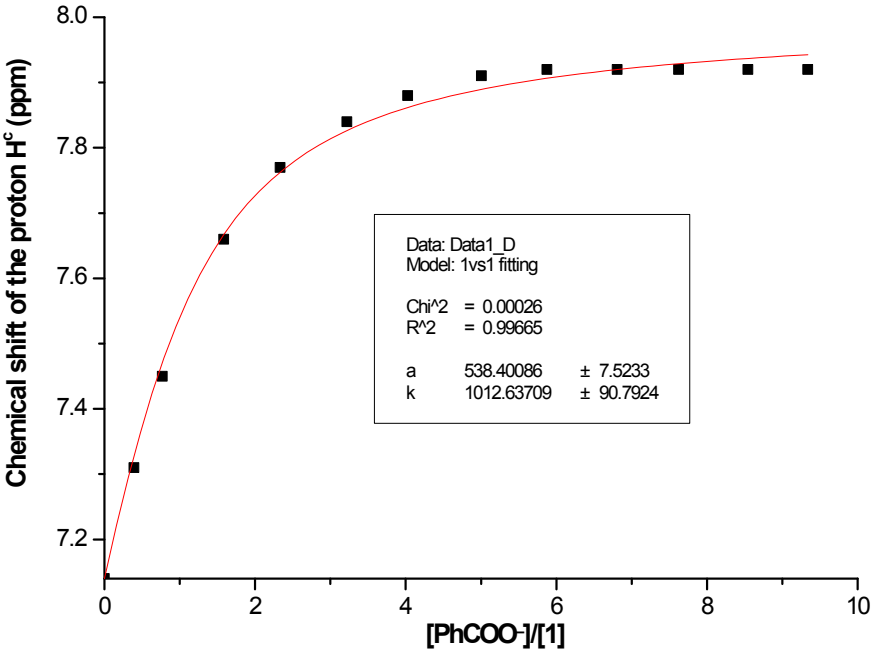

Figure S3. Fitting binding isotherms of macrocycle **1** with TBAPhCOO in CD_3CN at 298 K, showing chemical shift changes of the proton H^c based on a 1:1 binding model (K_a = 1013 M^{-1}).

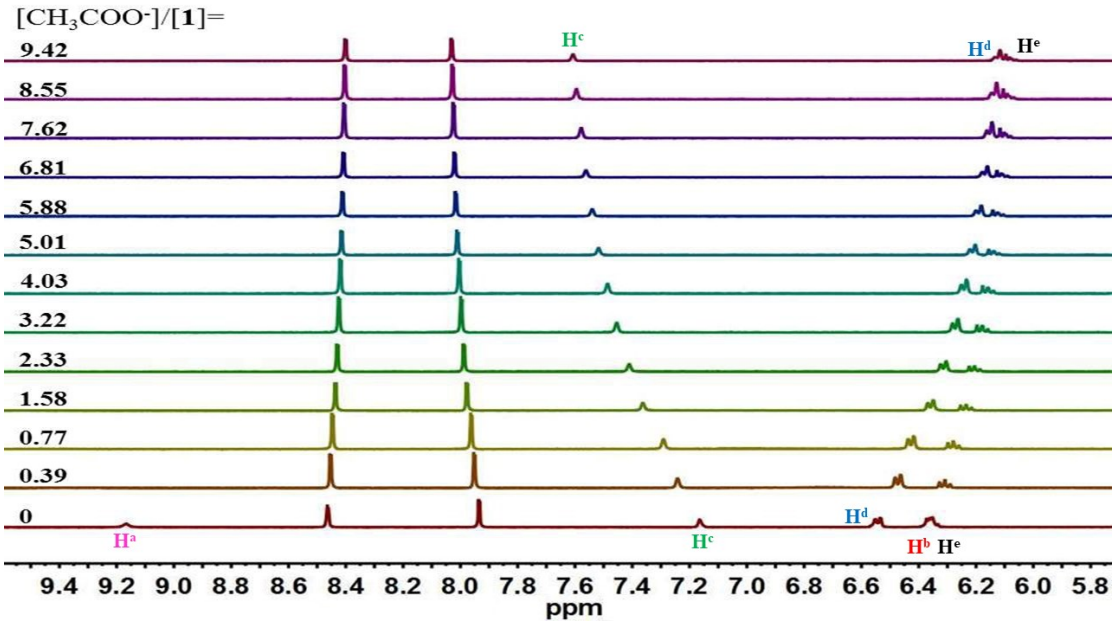

Figure S4. Stack plot of ^{1}H NMR titration of **1** (1.6 mM) with $TBACH_3COO$ in CD_3CN at 298 K.

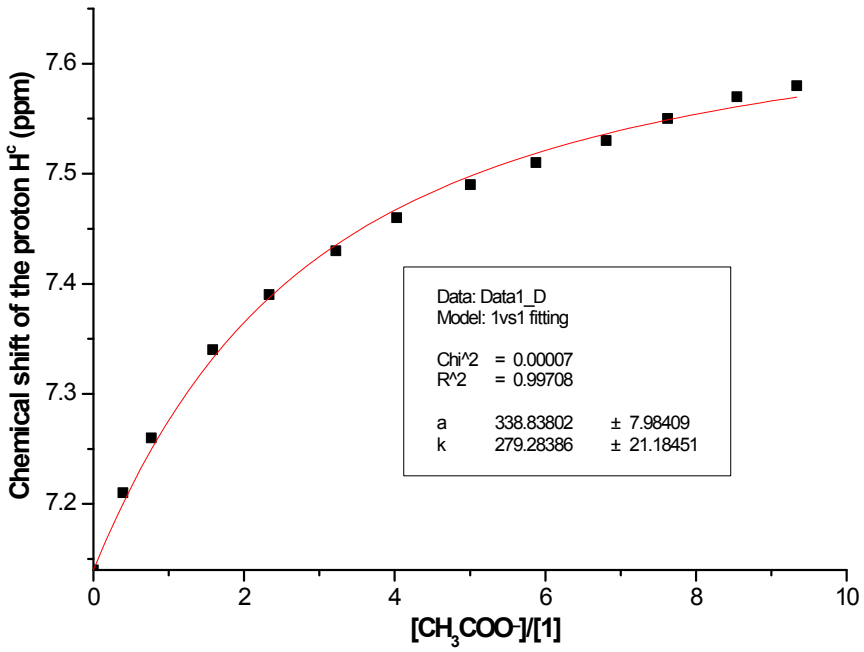

Figure S5. Fitting binding isotherms of macrocycle **1** with $TBACH_3COO$ in CD_3CN at 298 K, showing chemical shift changes of the proton H^c based on a 1:1 binding model (K_a = 279 M^{-1}).

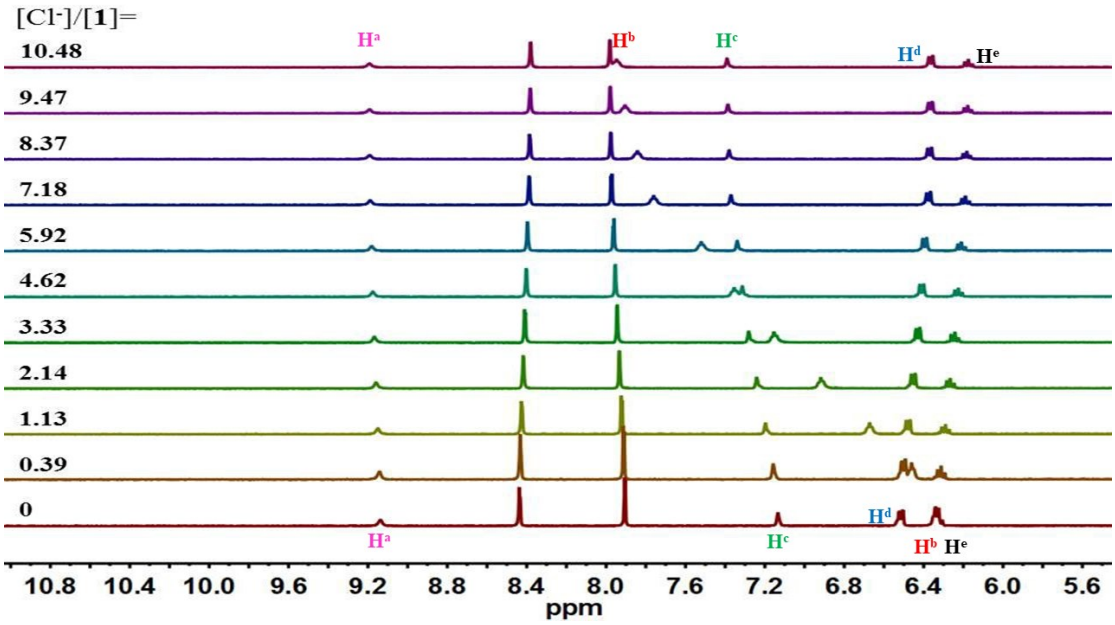

Figure S6. Stack plot of ^{1}H NMR titration of macrocycle **1** (1.6 mM) with TBACl in CD_3CN at 298 K.

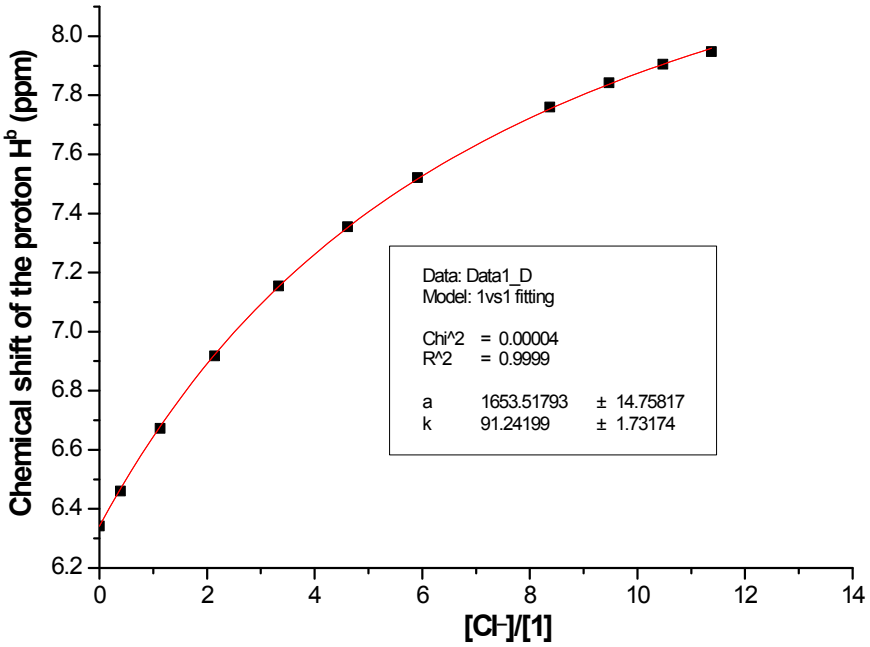

Figure S7. Fitting binding isotherms of macrocycle **1** with TBACl in CD_3CN at 298 K, showing chemical shift changes of the proton H^b based on a 1:1 binding model ($K_a = 91\ M^{-1}$).

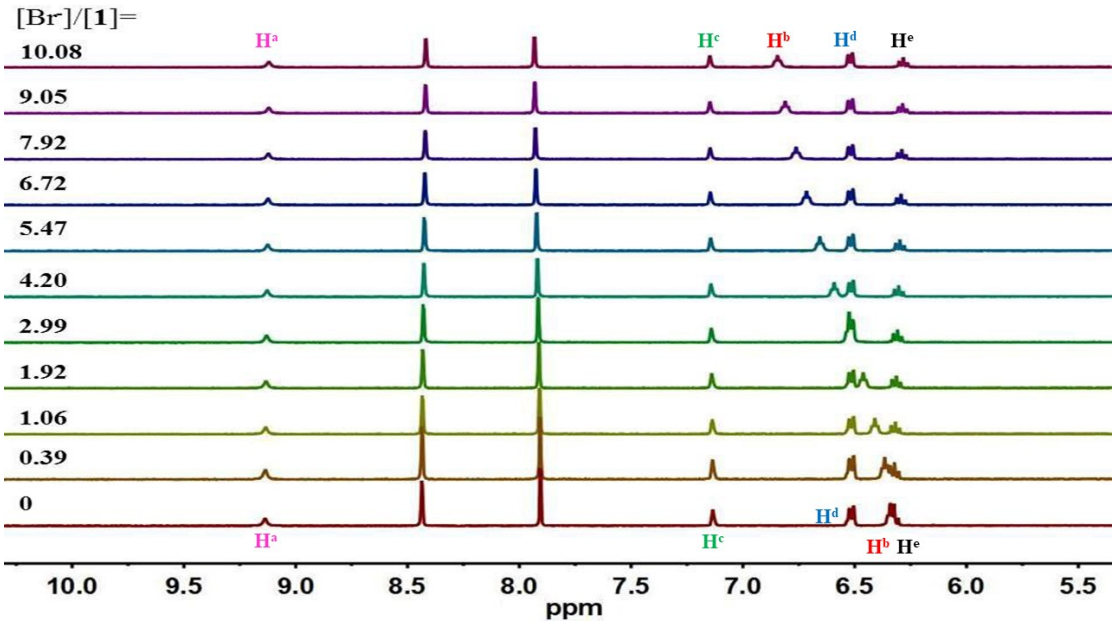

Figure S8. Stack plot of ^{1}H NMR titration of macrocycle **1** (1.6 mM) with TBABr in CD_3CN at 298 K.

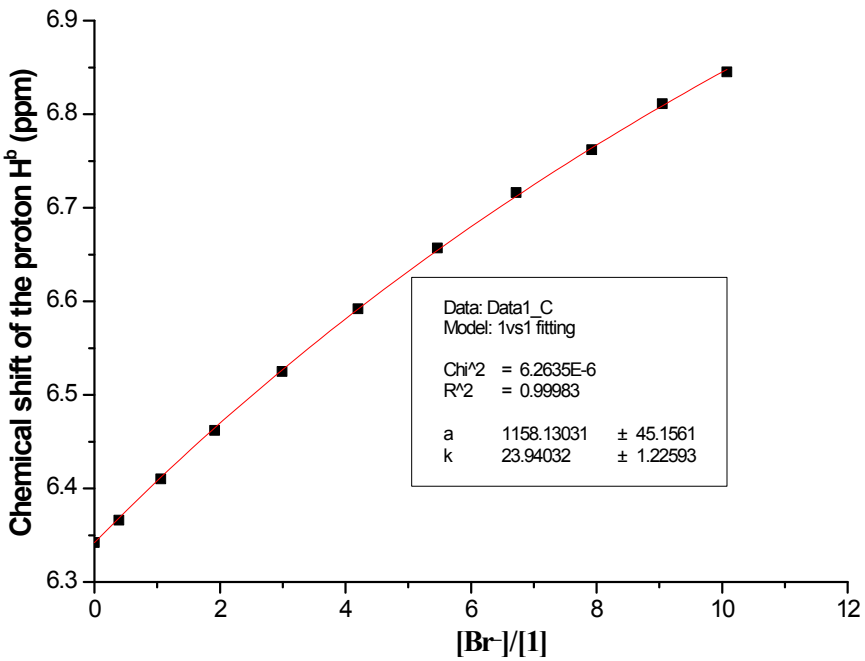

Figure S9. Fitting binding isotherms of macrocycle **1** with TBABr in CD_3CN at 298 K, showing chemical shift changes of the proton H^b based on a 1:1 binding model ($K_a = 24\ M^{-1}$).

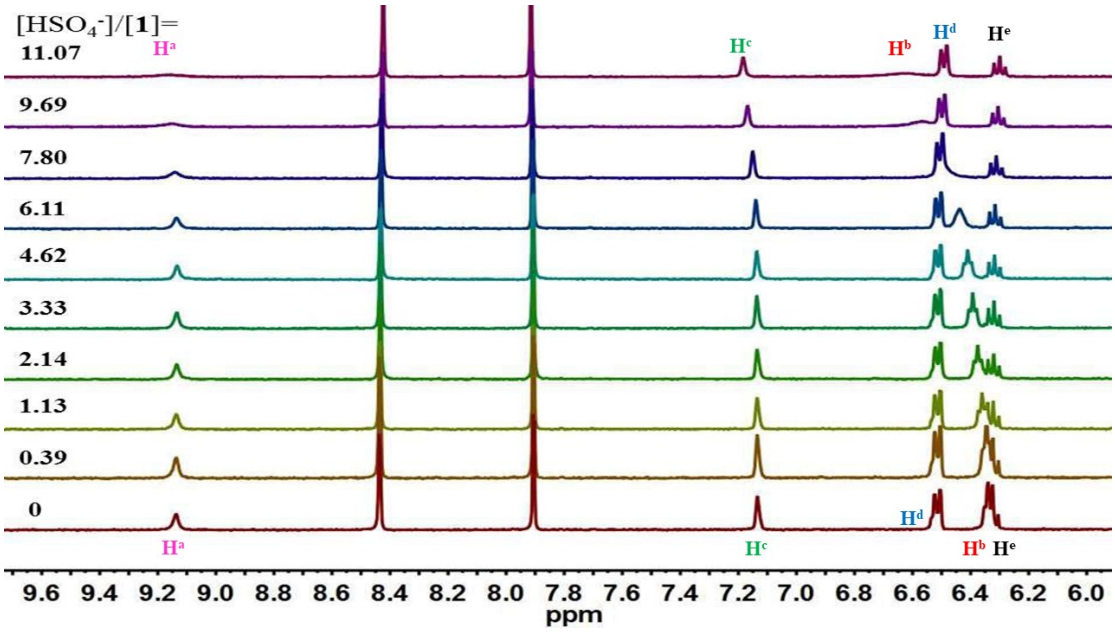

Figure S10. Stack plot of ^{1}H NMR titration of macrocycle **1** (1.6 mM) with $TBAHSO_4$ in CD_3CN at 298 K (K_a <10 M^{-1}).

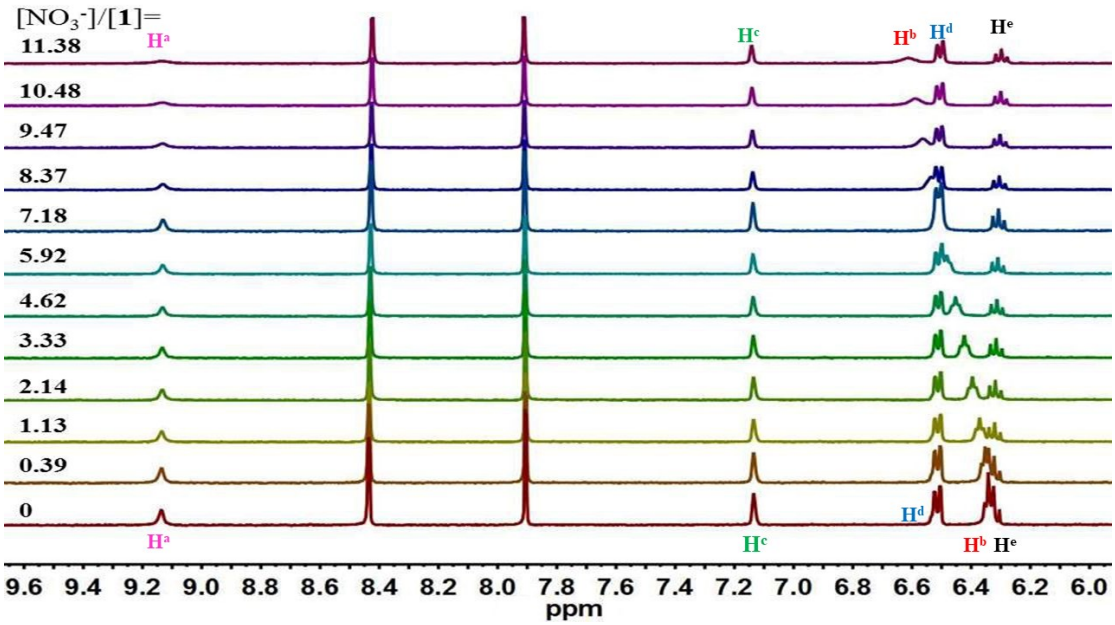

Figure S11. Stack plot of ^{1}H NMR titration of macrocycle **1** (1.6 mM) with $TBANO_3$ in CD_3CN at 298 K (K_a <10 M^{-1}).

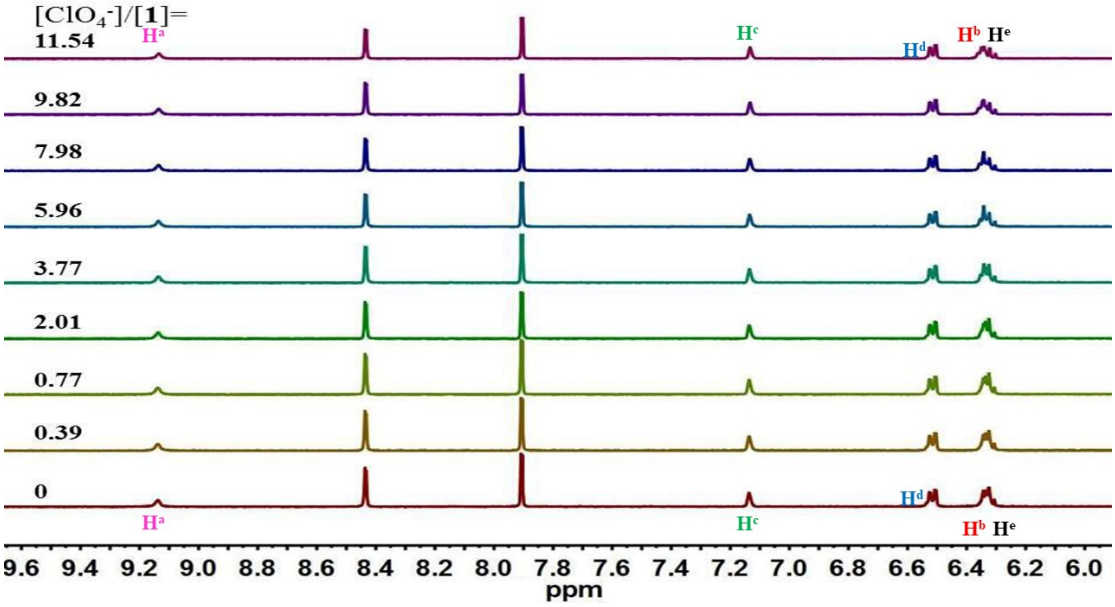

Figure S12. Stack plot of ^{1}H NMR titration of macrocycle **1** (1.6 mM) with $TBAClO_4$ in CD_3CN at 298 K (no binding).

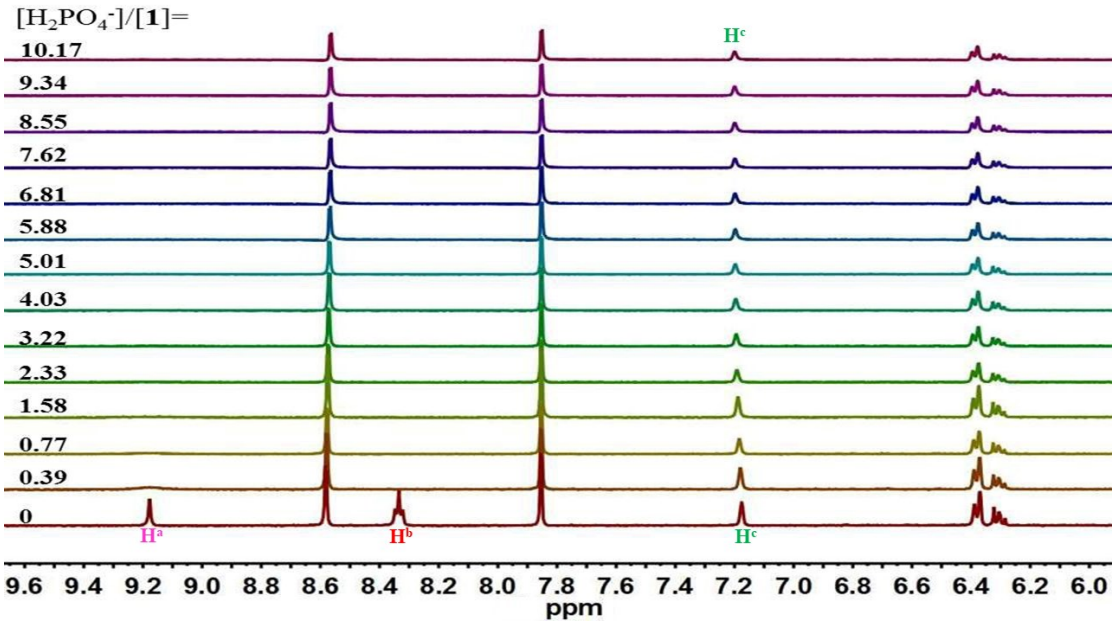

Figure S13. Stack plot of ^{1}H NMR titration of macrocycle **1** (1.6 mM) with $TBAH_2PO_4$ in DMSO-d_6 at 298 K (very weak or no binding).

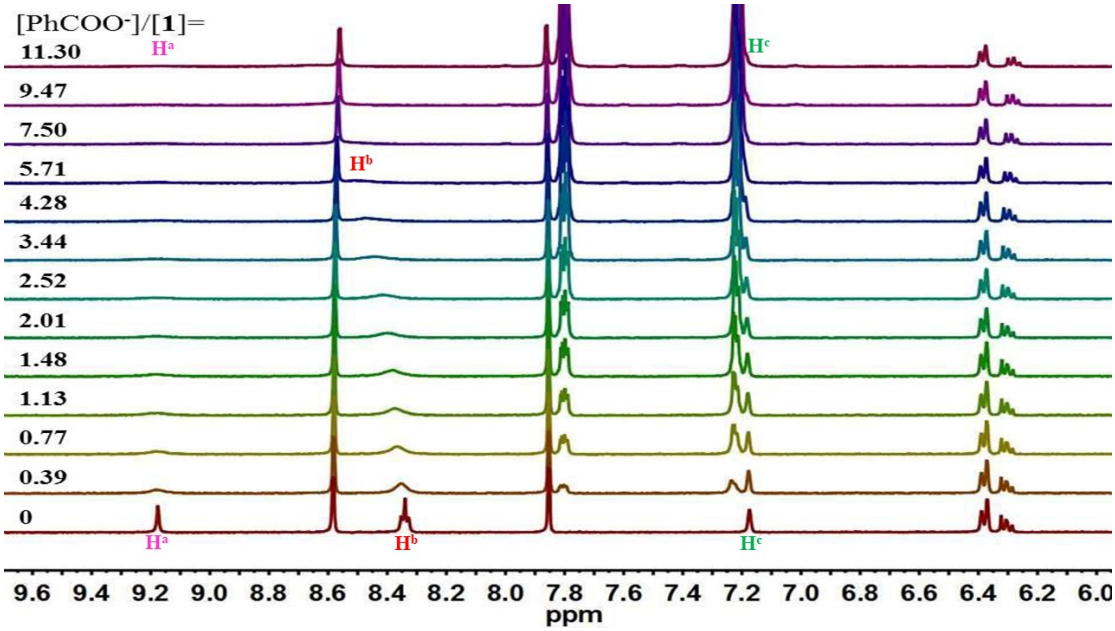

Figure S14. Stack plot of ^{1}H NMR titration of macrocycle **1** (1.6 mM) with TBAPhCOO in DMSO-d_6 at 298 K (very weak binding).

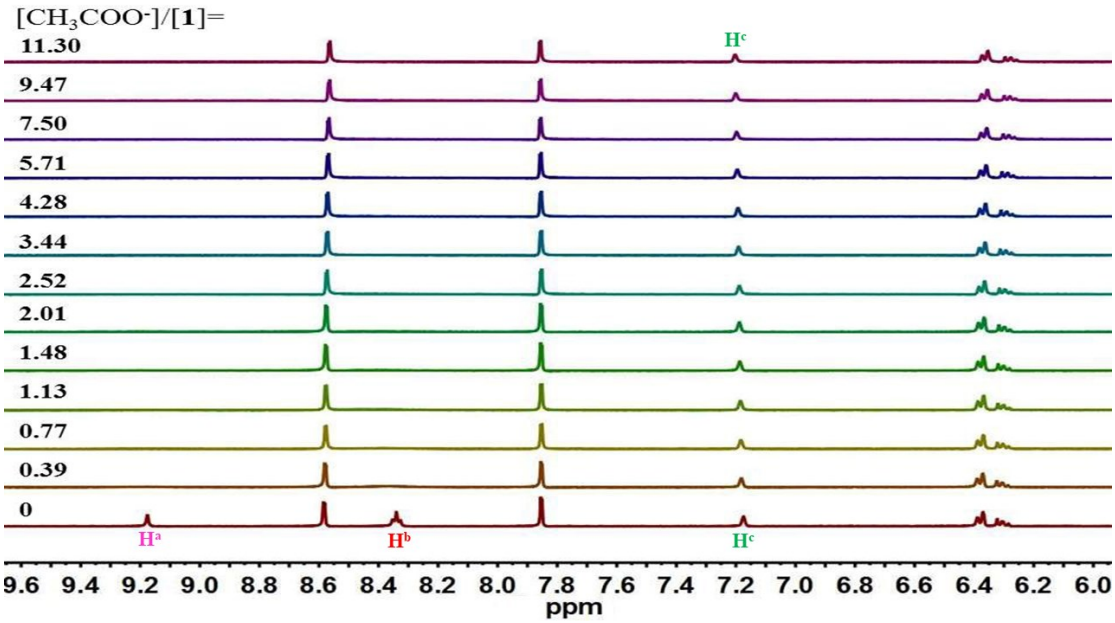

Figure S15. Stack plot of ^{1}H NMR titration of macrocycle **1** (1.6 mM) with $TBACH_3COO$ in DMSO-d_6 at 298 K (very weak or no binding).

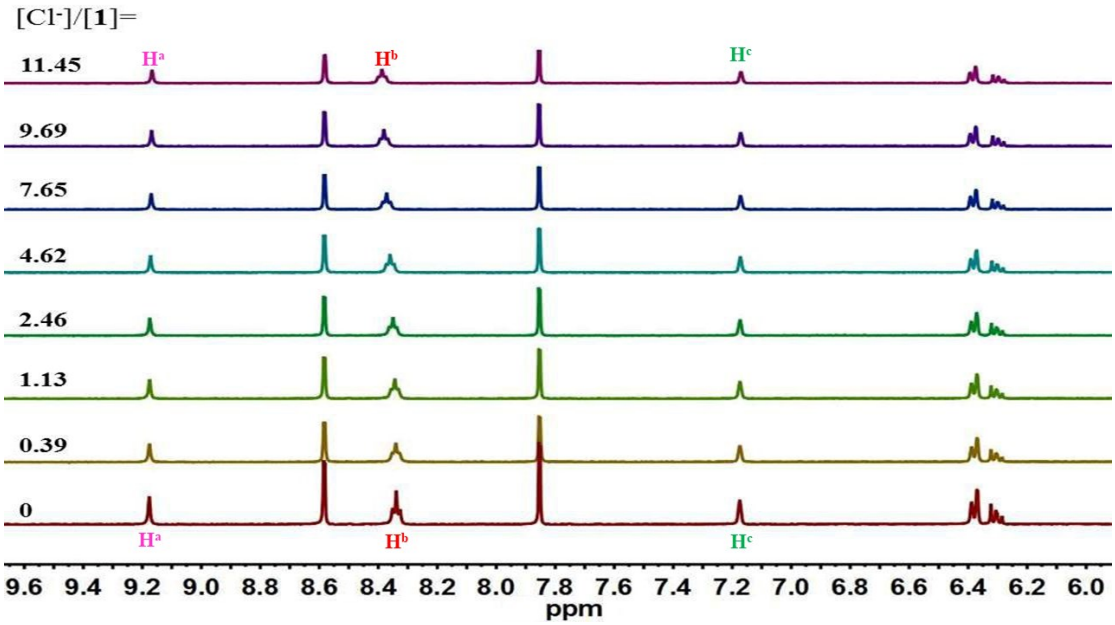

Figure S16. Stack plot of ^{1}H NMR titration of macrocycle **1** (1.6 mM) with TBACl in DMSO-d_6 at 298 K (no binding).

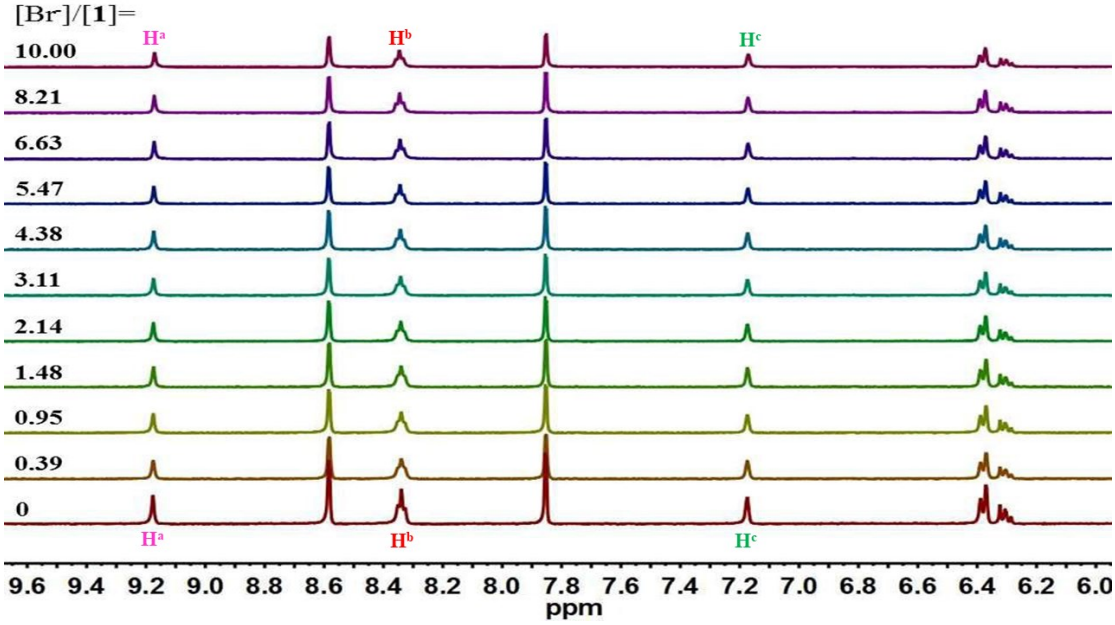

Figure S17. Stack plot of ^{1}H NMR titration of macrocycle **1** (1.6 mM) with TBABr in DMSO-d_6 at 298 K (no binding).

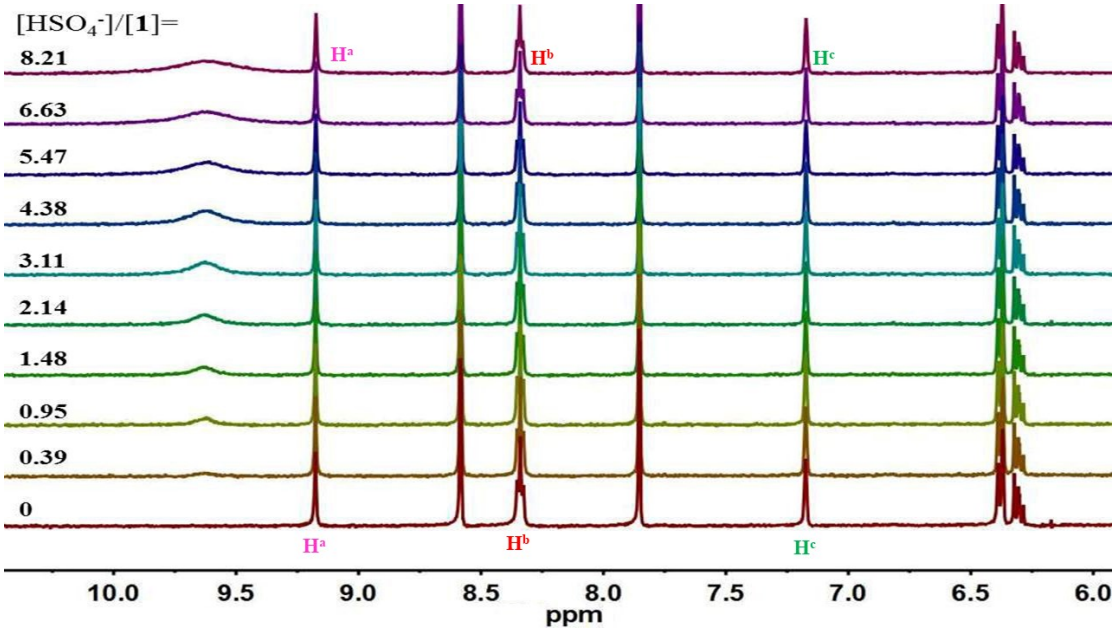

Figure S18. Stack plot of ^{1}H NMR titration of macrocycle **1** (1.6 mM) with $TBAHSO_4$ in DMSO-d_6 at 298 K (no binding).

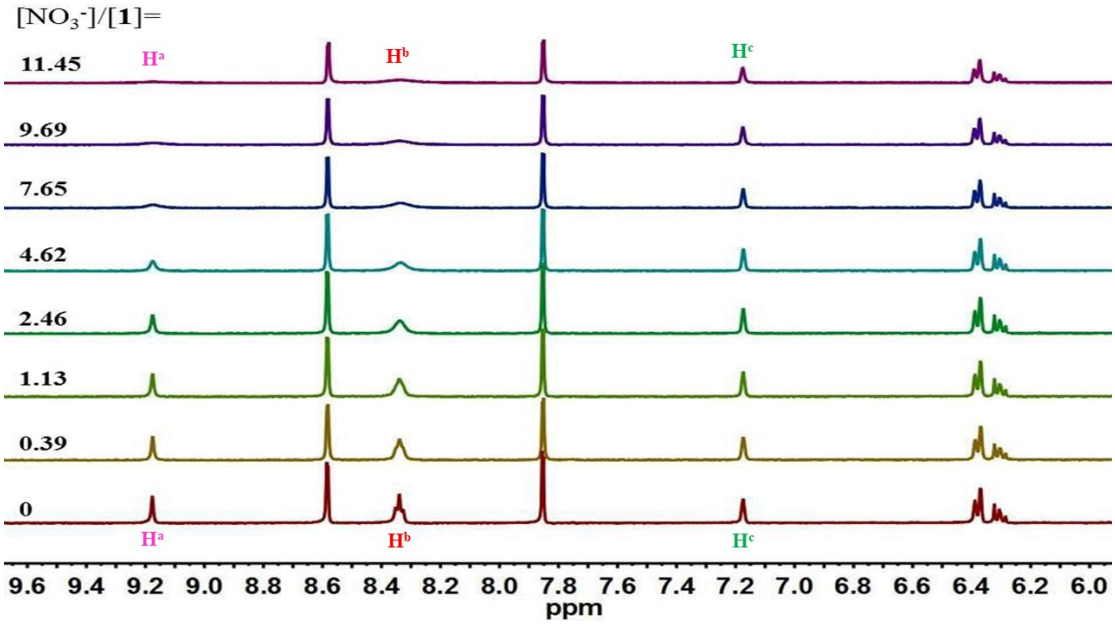

Figure S19. Stack plot of ^{1}H NMR titration of macrocycle **1** (1.6 mM) with $TBANO_3$ in DMSO-d_6 at 298 K (very weak binding).

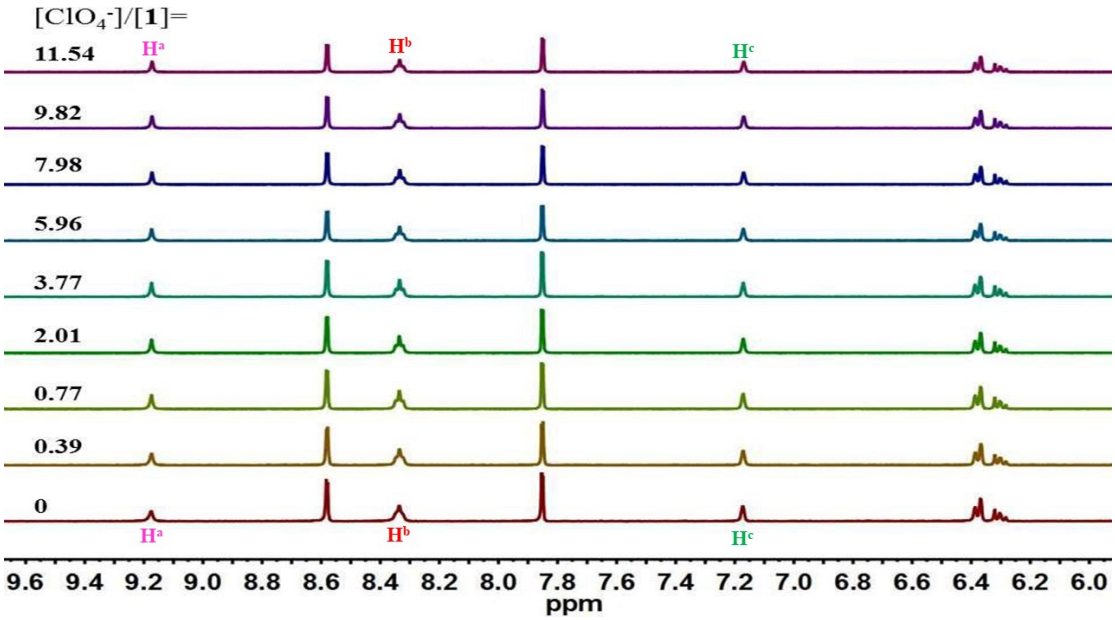

Figure S20. Stack plot of ^{1}H NMR titration of macrocycle **1** (1.6 mM) with $TBAClO_4$ in DMSO-d_6 at 298 K (no binding).

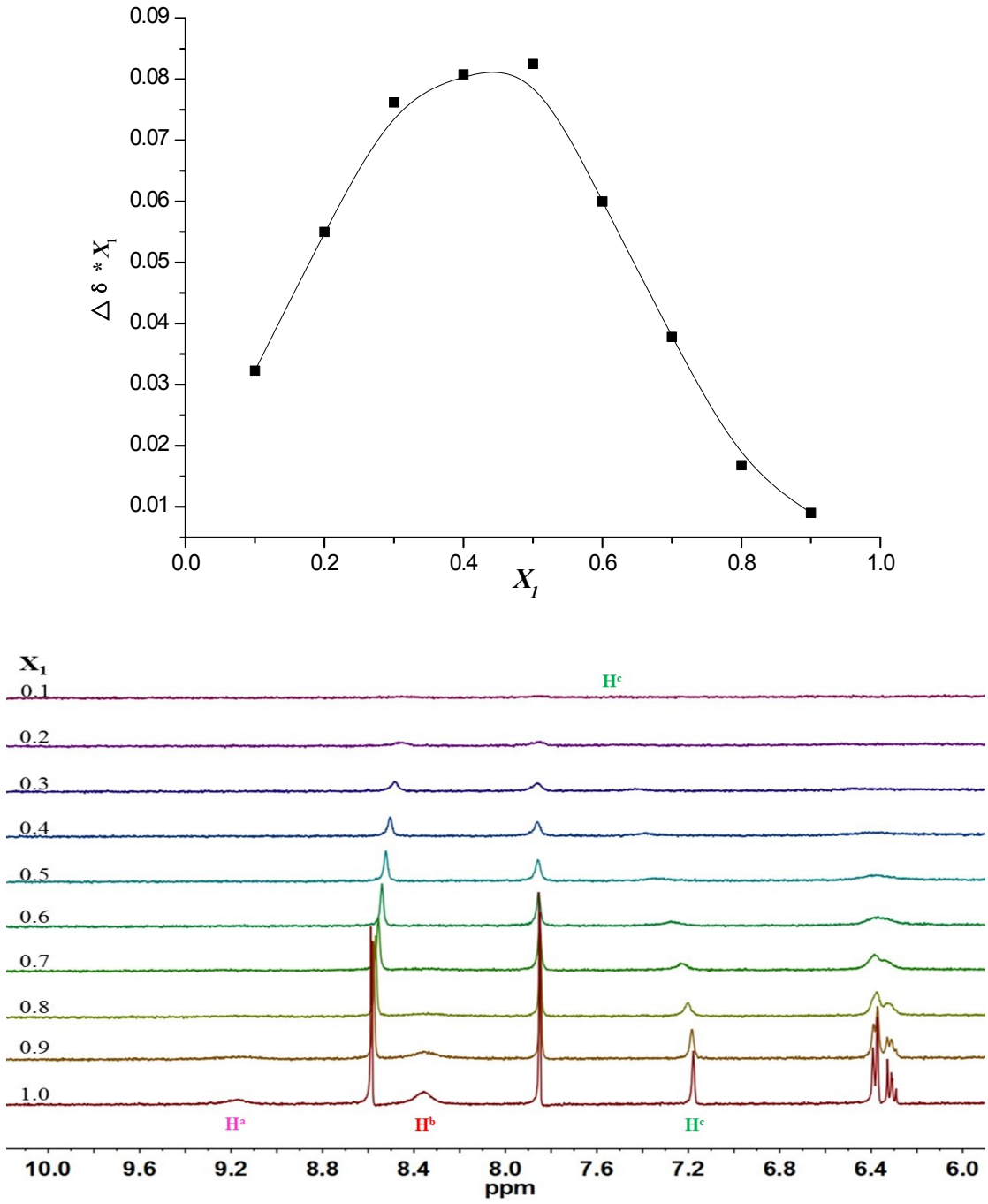

Figure S21. Job's plot of macrocycle **1** with TBAF (monitoring the chemical shift of the proton H^c) in DMSO-d_6 at 298 K with a total concentration of 1.0 mM (top) and the corresponding ^1H NMR spectra (bottom).

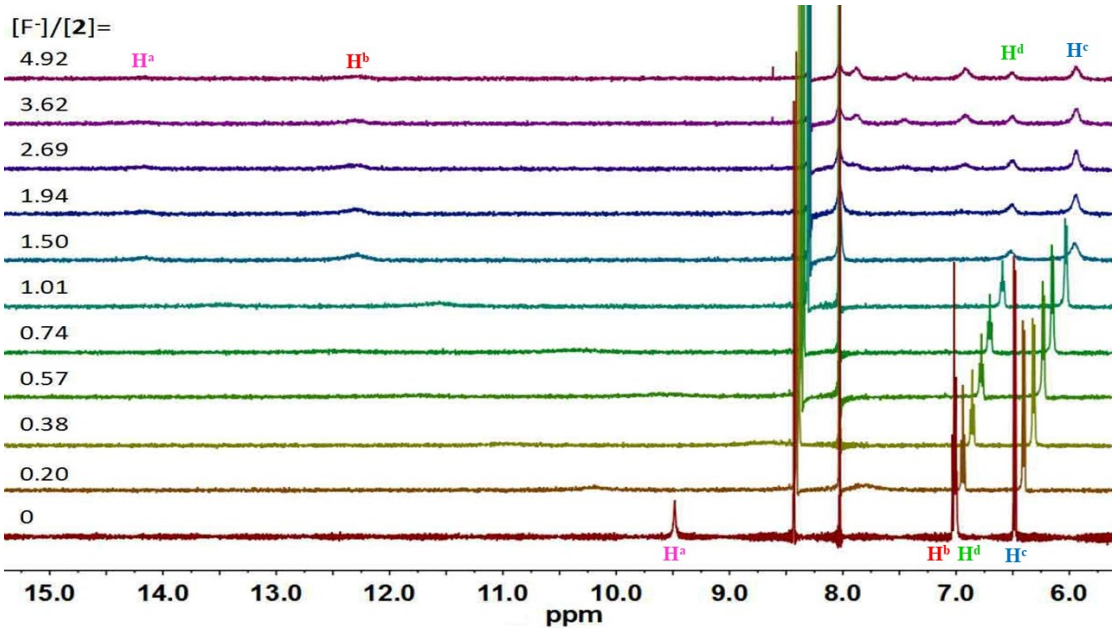

Figure S22. Stack plot of ^{1}H NMR titration of macrocycle **2** (1.6 mM) with TBAF in CD_3CN at 298 K.

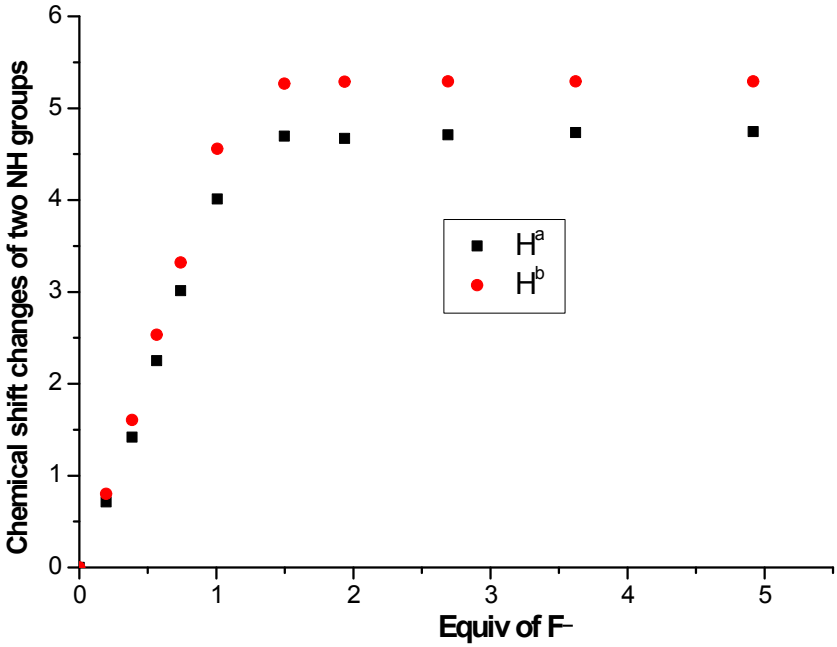

Figure S23. Chemical shift changes of two NH groups in macrocycle **2** in CD_3CN upon addition of TBAF. An inflection point for the titration isotherm was seen at nearly 1.0 equiv of TBAF., indicative of a K_a >10000 M^{-1}.

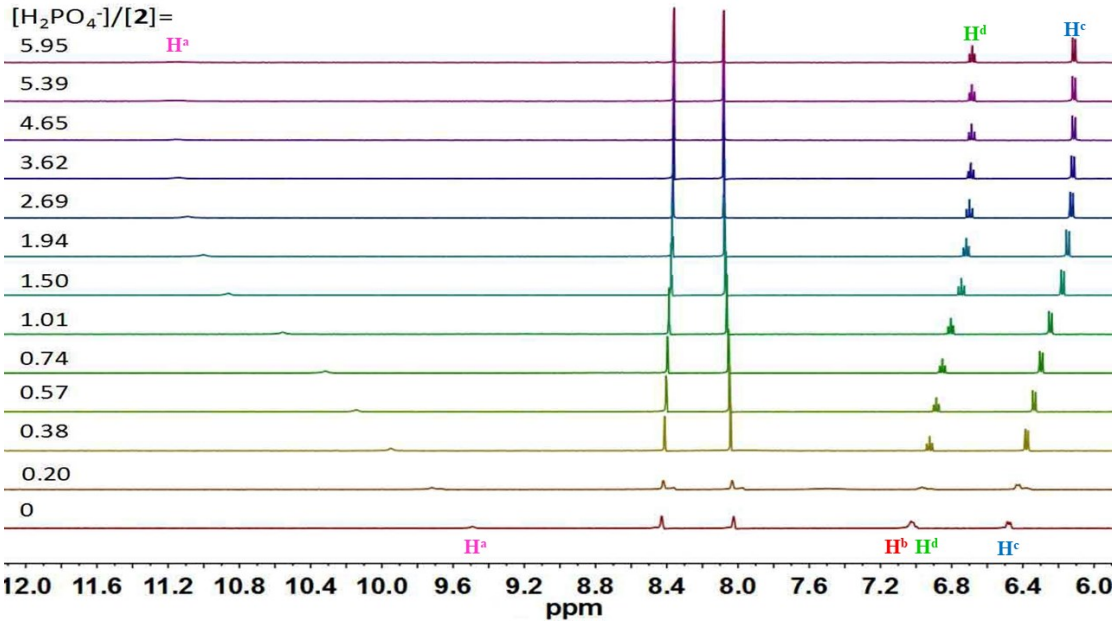

Figure S24. Stack plot of ^{1}H NMR titration of macrocycle **2** (1.6 mM) with $TBAH_2PO_4$ in CD_3CN at 298 K.

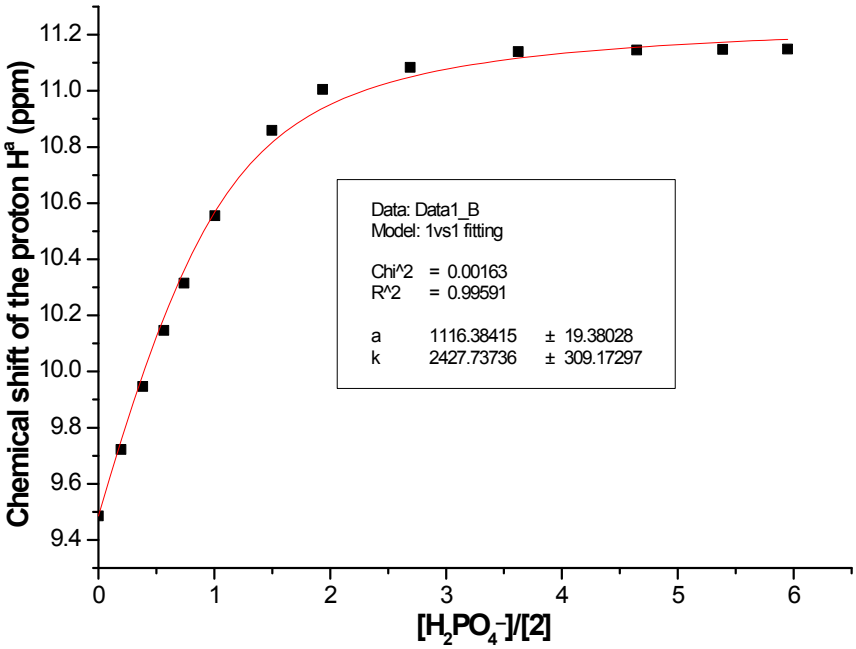

Figure S25. Fitting binding isotherms of macrocycle **2** with $TBAH_2PO_4$ in CD_3CN at 298 K, showing chemical shift changes of the proton H^a based on a 1:1 binding model (K_a = 2428 M^{-1}).

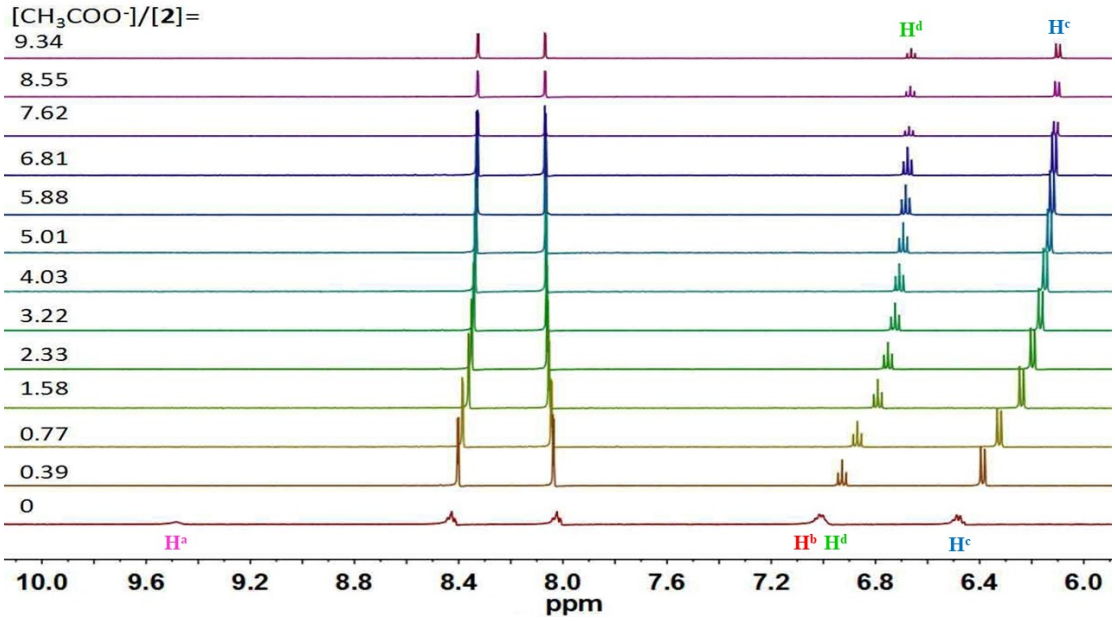

Figure S26. Stack plot of ^{1}H NMR titration of **2** (1.6 mM) with $TBACH_3COO$ in CD_3CN at 298 K.

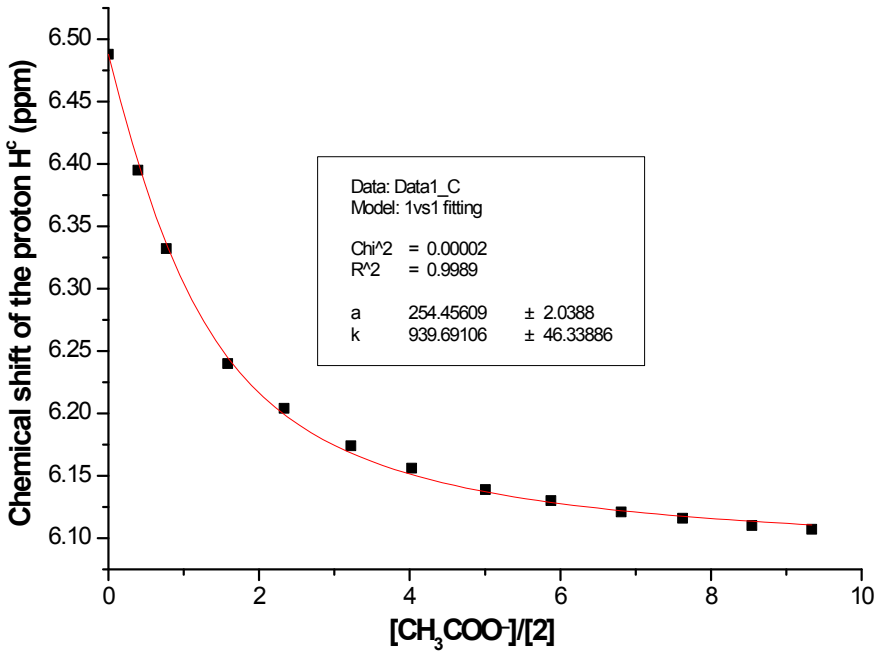

Figure S27. Fitting binding isotherms of macrocycle **2** with $TBACH_3COO$ in CD_3CN at 298 K, showing chemical shift changes of the proton H^c based on a 1:1 binding model (K_a = 939 M^{-1}).

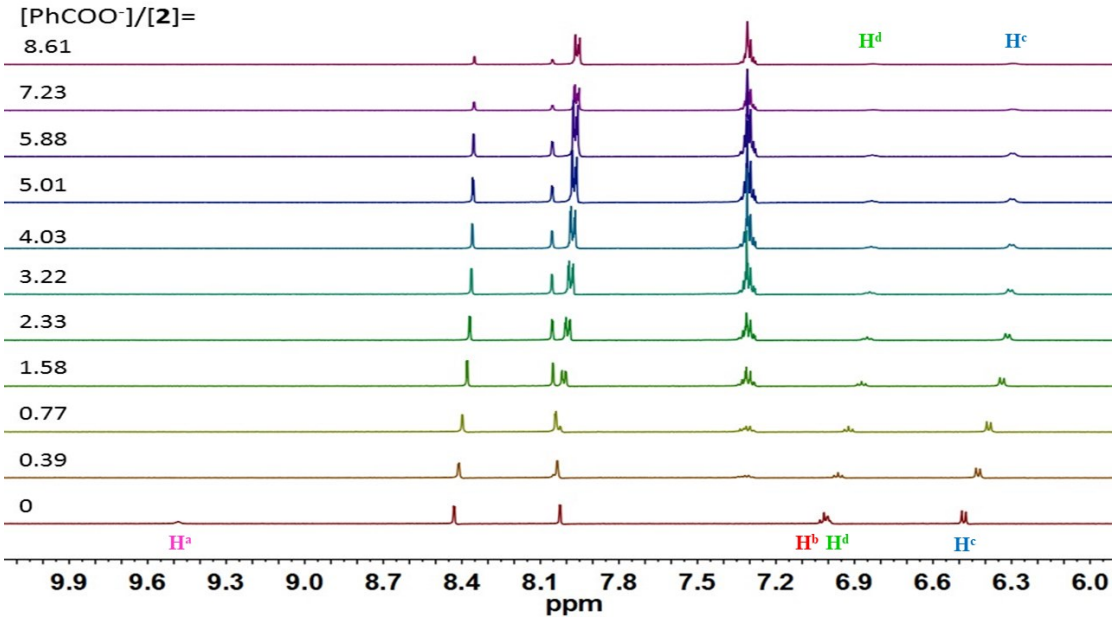

Figure S28. Stack plot of ^{1}H NMR titration of **2** (1.6 mM) with TBAPhCOO in CD_3CN at 298 K.

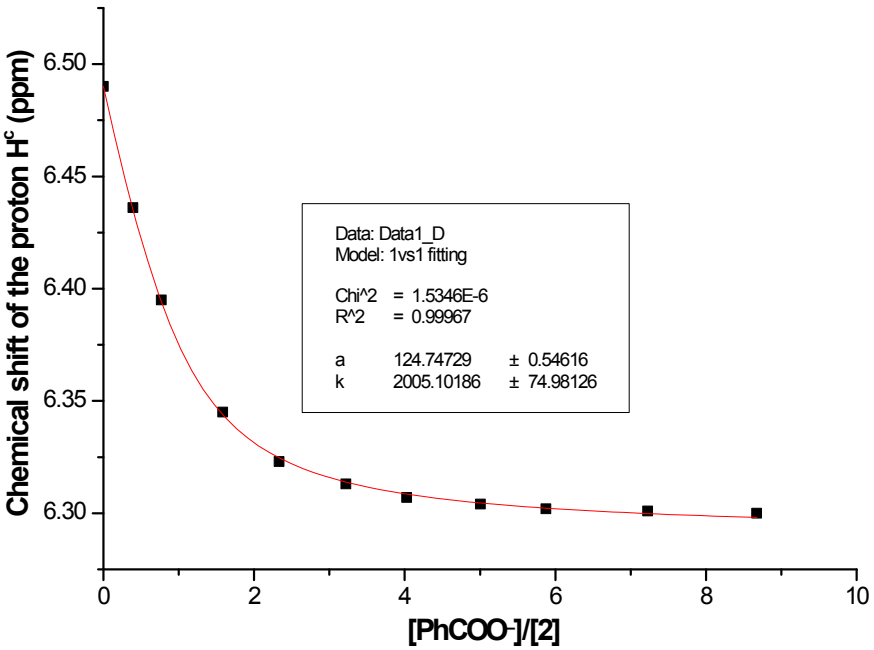

Figure S29. Fitting binding isotherms of macrocycle **2** with TBAPhCOO in CD_3CN at 298 K, showing chemical shift changes of the proton H^c based on a 1:1 binding model (K_a = 2005 M^{-1}).

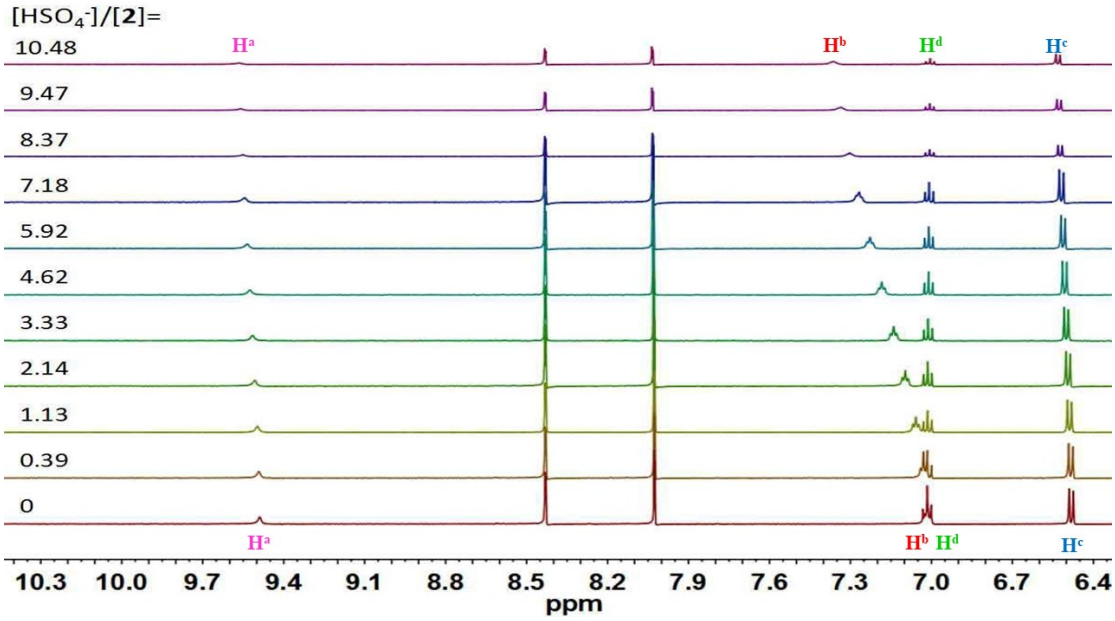

Figure S30. Stack plot of ^{1}H NMR titration of macrocycle **2** (1.6 mM) with $TBAHSO_4$ in CD_3CN at 298 K.

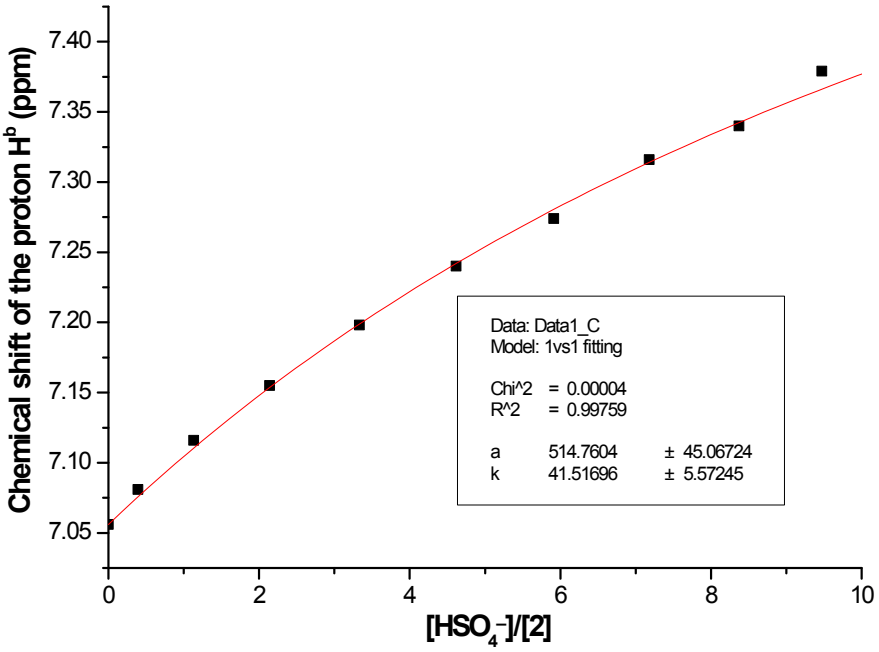

Figure S31. Fitting binding isotherms of macrocycle **2** with $TBAHSO_4$ in CD_3CN at 298 K, showing chemical shift changes of the proton H^b based on a 1:1 binding model (K_a = 41 M^{-1}).

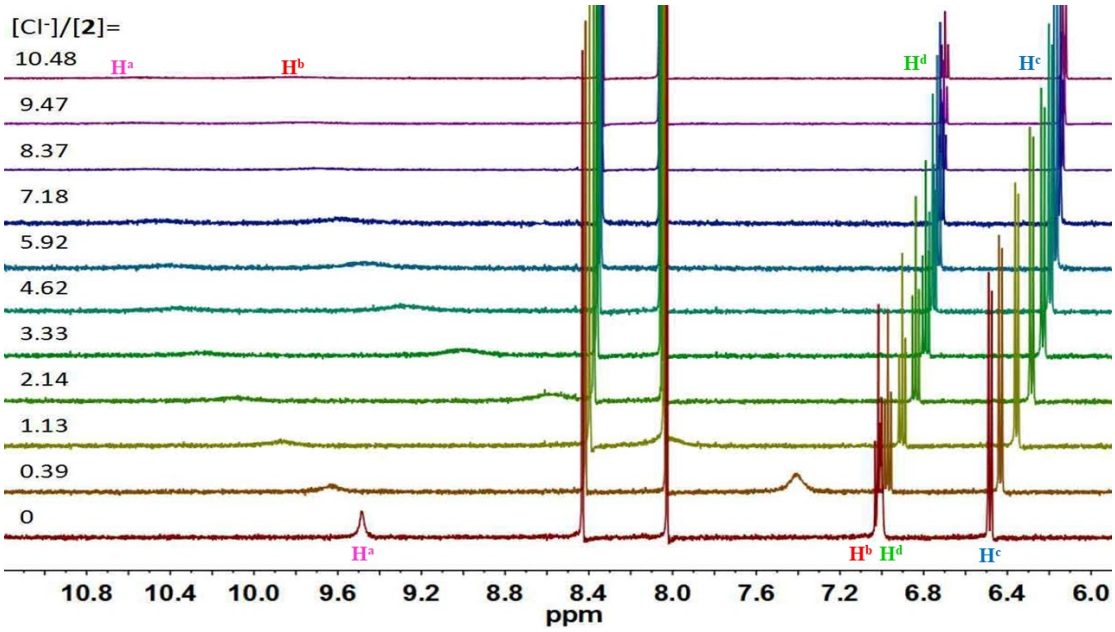

Figure S32. Stack plot of ^{1}H NMR titration of macrocycle **2** (1.6 mM) with TBACl in CD_3CN at 298 K.

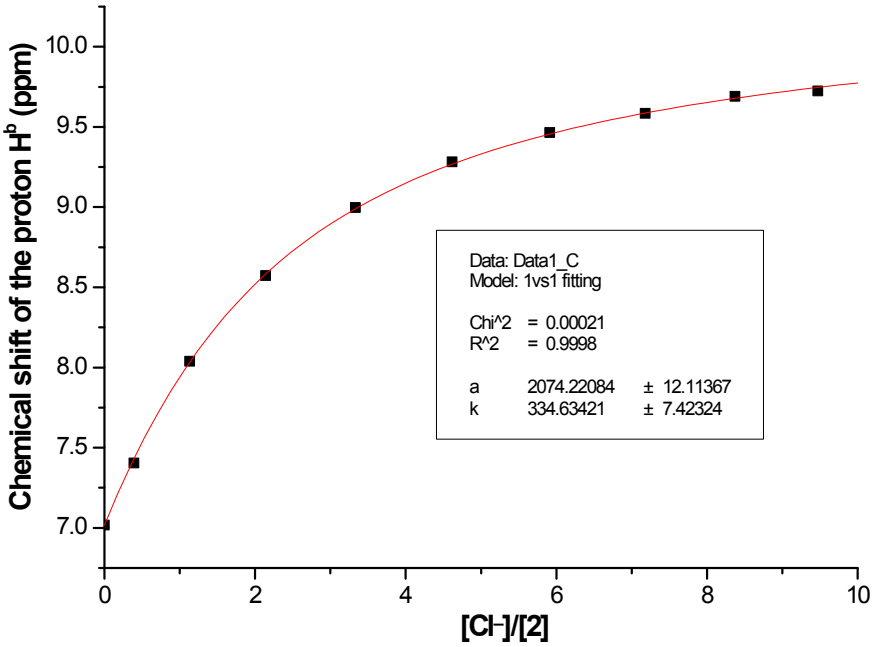

Figure S33. Fitting binding isotherms of macrocycle **2** with TBACl in CD_3CN at 298 K, showing chemical shift changes of the proton H^b based on a 1:1 binding model (K_a = 334 M^{-1}).

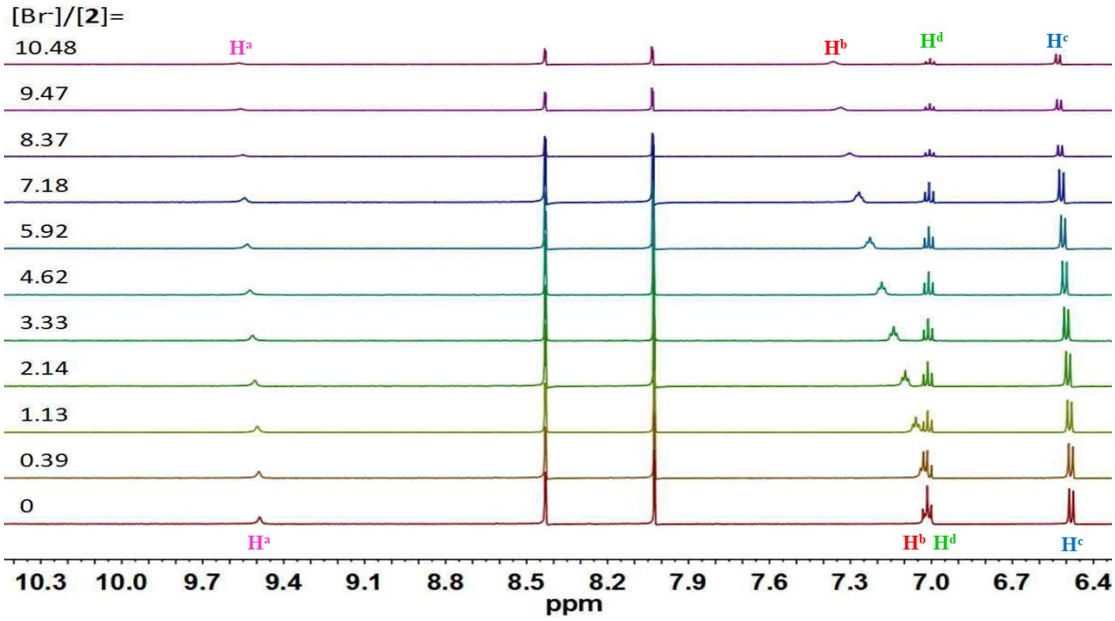

Figure S34. Stack plot of ^{1}H NMR titration of macrocycle **2** (1.6 mM) with TBABr in CD_3CN at 298 K (K_a <10 M^{-1}).

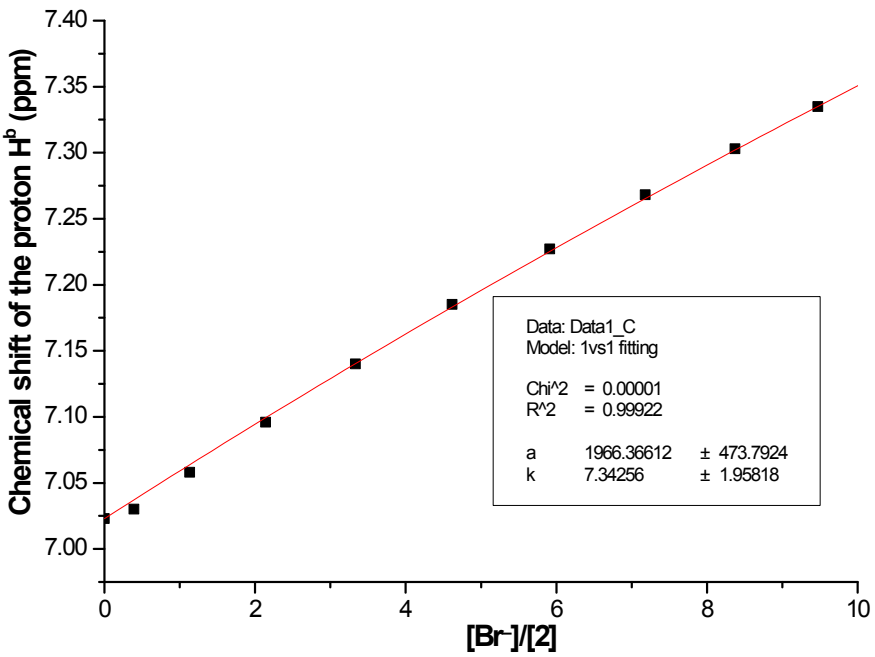

Figure S35. Fitting binding isotherms of macrocycle **2** with TBABr in CD_3CN at 298 K, showing chemical shift changes of the proton H^b based on a 1:1 binding model (K_a = 7 M^{-1}).

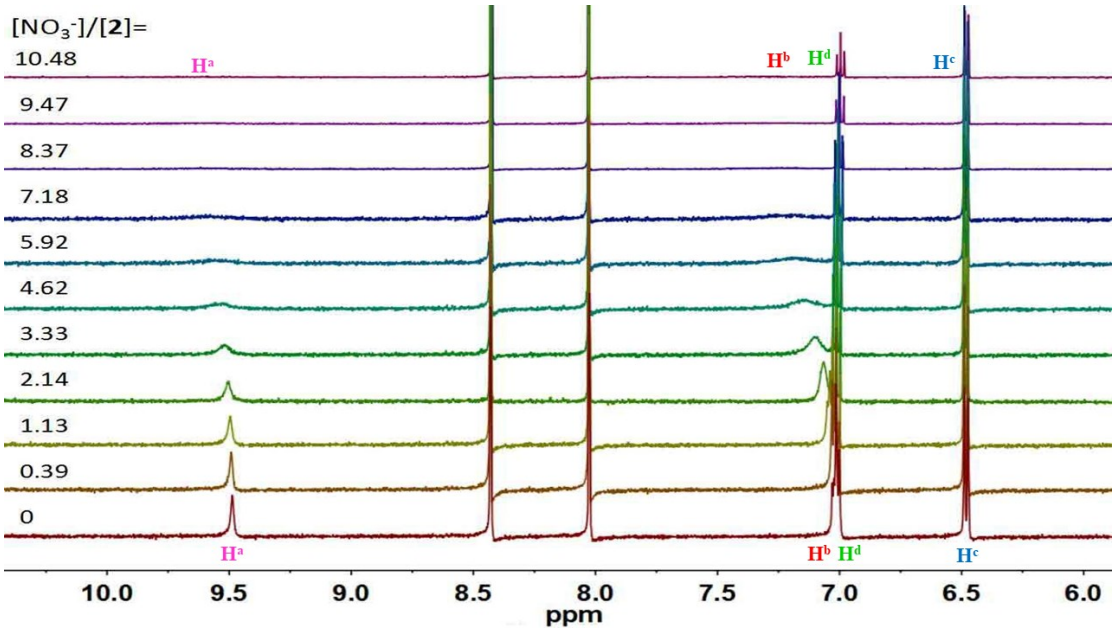

Figure S36. Stack plot of ^{1}H NMR titration of macrocycle **2** (1.6 mM) with $TBANO_3$ in CD_3CN at 298 K (K_a <10 M^{-1}).

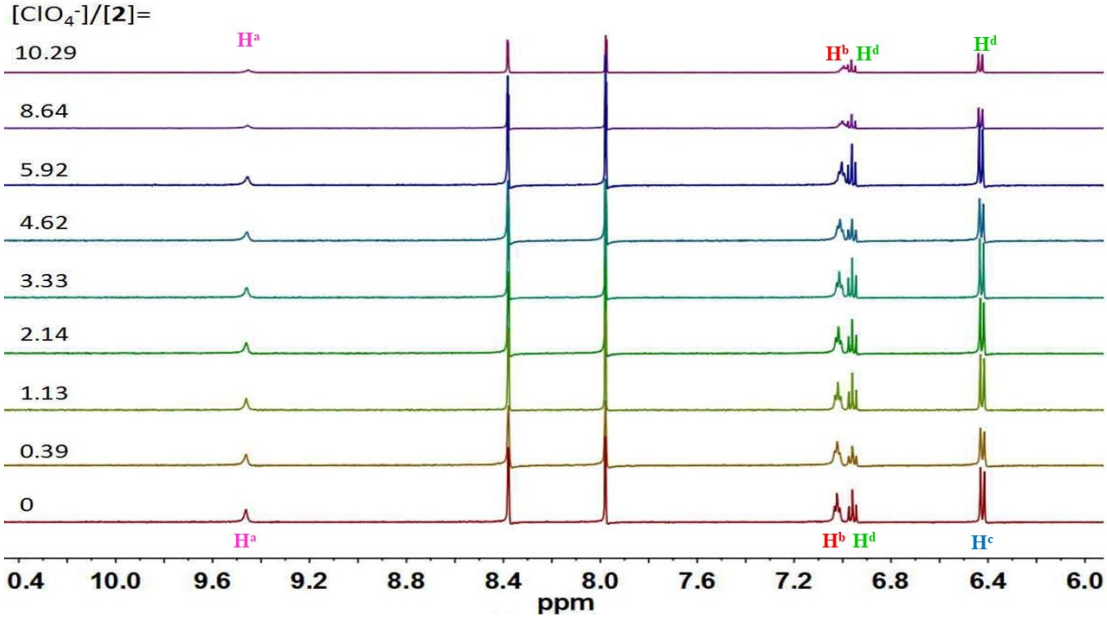

Figure S37. Stack plot of ^{1}H NMR titration of macrocycle **2** (1.6 mM) with $TBAClO_4$ in CD_3CN at 298 K (no binding).

3. UV-vis titration studies

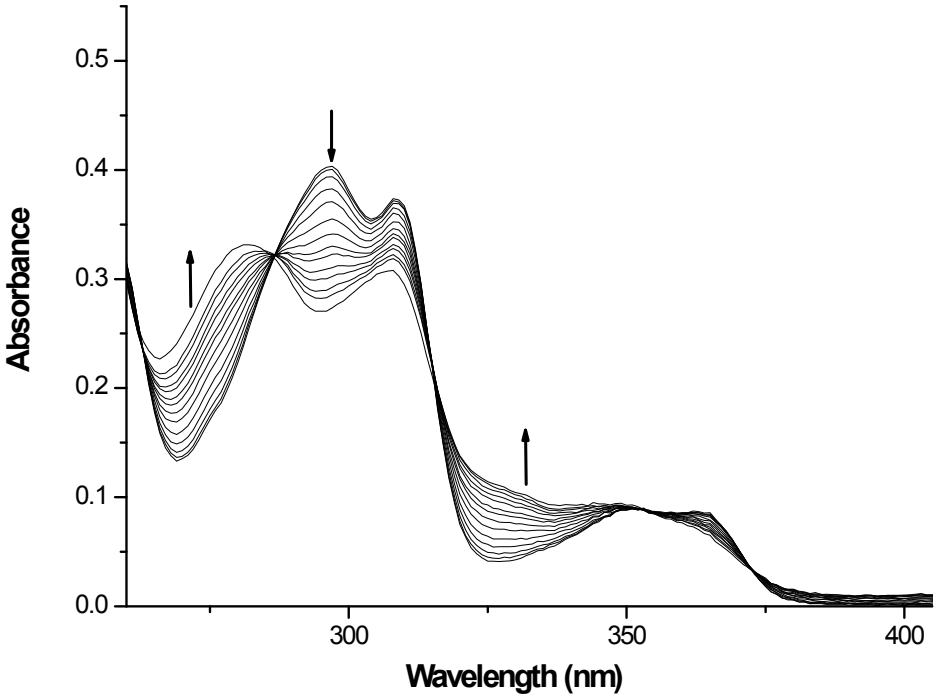

Figure S38. UV-vis titration of macrocycle **1** (20 μM) with strong base TBAOH (0~17.3 equiv) in CH_3CN.

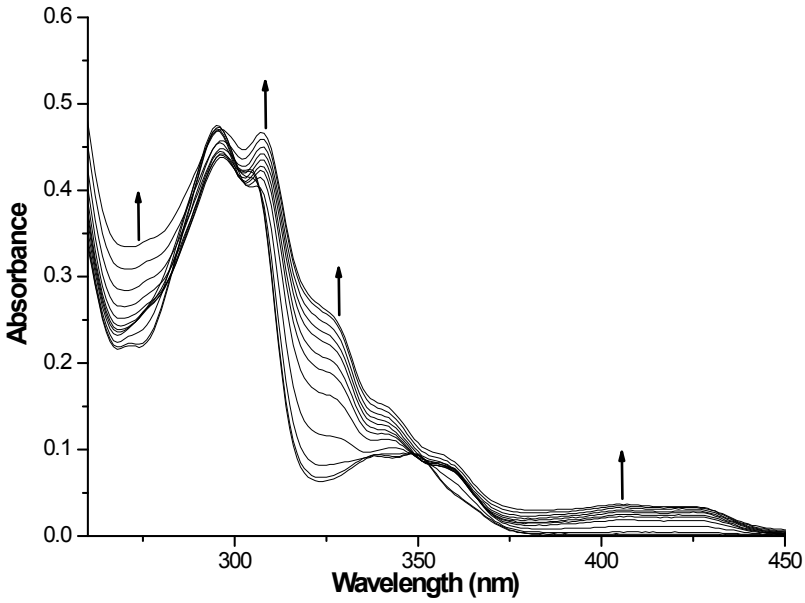

Figure S39. UV-vis spectral changes of macrocycle **2** (20 μM) in CH_3CN upon addition of TBAF (0~ 63 equiv).

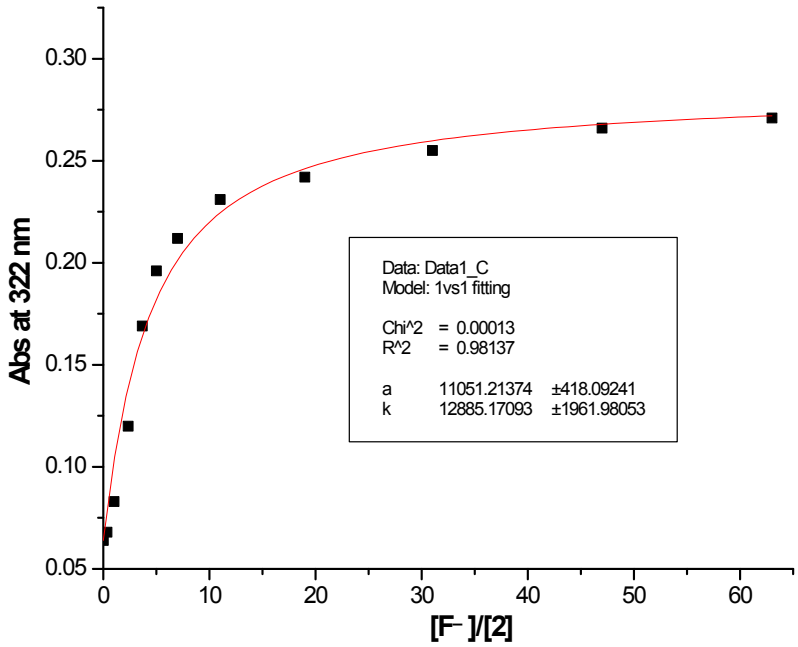

Figure S40. A 1:1 non-linear curve fitting of the absorbance at 322 nm of macrocycle **2** against the added F^- (K_a = 12885 M^{-1}).

4. Cartesian coordinates

B3LYP/6-311++G(d,p) Energy: -347.934691 Hartree
Num. Imaginary Frequencies: 0
Cartesian Coordinates (Angstroms) for the Optimized Structures of the **1**/F^- Complex in Acetonitrile

C	3.232786	-2.476024	-0.218567
C	2.001376	-3.116263	-0.012446
C	0.809406	-2.415527	0.200390
C	0.831854	-1.015368	0.180691
C	2.078187	-0.355270	0.002293
C	3.252635	-1.076205	-0.189907
N	-0.184925	-0.074612	0.272676
C	0.388796	1.181441	0.191466
C	1.795709	1.067476	0.061668
C	-0.192709	2.458765	0.177533
C	0.643085	3.580591	0.173258
C	2.042979	3.480346	0.131767
C	2.603281	2.201323	0.028569
C	2.955631	4.721321	0.154678
C	3.903521	4.632392	1.373866
C	2.156843	6.032958	0.262789
C	3.794573	4.772230	-1.143546
C	4.537114	-3.259347	-0.460639
C	5.129324	-2.858568	-1.832188
C	4.314345	-4.782681	-0.461368
C	5.554006	-2.920798	0.654533
S	-0.605891	-3.437587	0.691721
S	-1.883558	2.787235	-0.355459
C	-3.856954	-1.754182	-0.863602
C	-5.153692	-2.256727	-0.745948
C	-6.198219	-1.391816	-0.409987
C	-5.941886	-0.051120	-0.119144
C	-4.644594	0.461373	-0.234260
C	-3.637583	-0.391056	-0.672937
C	-2.634168	-2.635854	-0.985925
C	-4.317862	1.877844	0.214308
N	-2.039618	-2.700107	0.377345
N	-2.929631	2.049513	0.716903
O	-2.121254	4.239547	-0.274260
O	-2.018899	2.211854	-1.712382
O	-0.548586	-4.663857	-0.118062
O	-0.531003	-3.559228	2.156790
H	-2.634543	-0.012363	-0.797700

H	1.950590	-4.195490	-0.010121
H	4.184552	-0.539459	-0.324749
H	-1.031944	-0.223178	0.883528
H	0.167461	4.549844	0.158958
H	3.676325	2.081812	-0.066738
H	4.531442	3.738962	1.335508
H	3.335486	4.605841	2.308128
H	4.564113	5.504190	1.402017
H	1.496007	6.181383	-0.595655
H	1.552073	6.068062	1.173217
H	2.849959	6.877638	0.293919
H	4.424879	3.886964	-1.256640
H	4.450119	5.648219	-1.133604
H	3.147956	4.841288	-2.022858
H	4.432143	-3.093700	-2.641436
H	5.355295	-1.790711	-1.881015
H	6.059403	-3.405183	-2.014979
H	3.622126	-5.093590	-1.248790
H	3.928385	-5.139940	0.497317
H	5.266810	-5.287929	-0.641429
H	6.488020	-3.466757	0.490789
H	5.791481	-1.854573	0.678646
H	5.163311	-3.202077	1.636562
H	-5.345734	-3.315255	-0.885349
H	-7.208249	-1.776249	-0.321970
H	-6.750032	0.588060	0.222524
H	-1.927246	-2.213095	-1.707849
H	-2.892118	-3.645784	-1.303799
H	-4.490730	2.596190	-0.591611
H	-4.993922	2.160682	1.024332
H	-2.206376	-1.883446	0.990880
H	-2.561708	1.199493	1.188788
F	-2.157075	-0.333536	1.894640

5. Original Spectral Files of Macrocyles 1 and 2

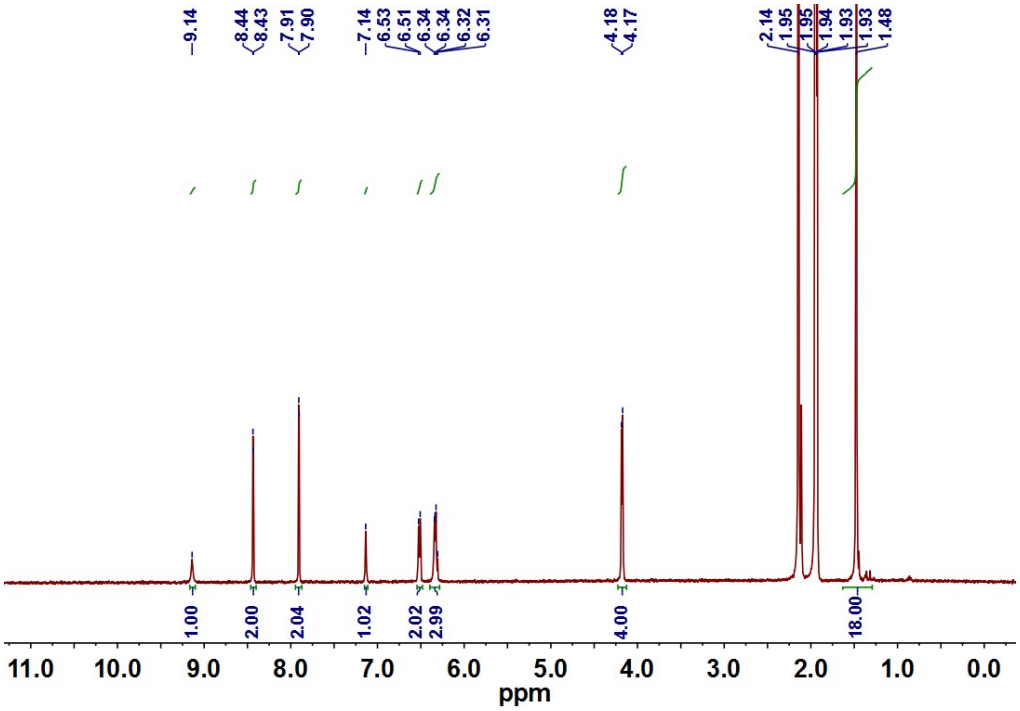

Figure S41. ^{1}H NMR spectrum of macrocycle **1** in CD_3CN.

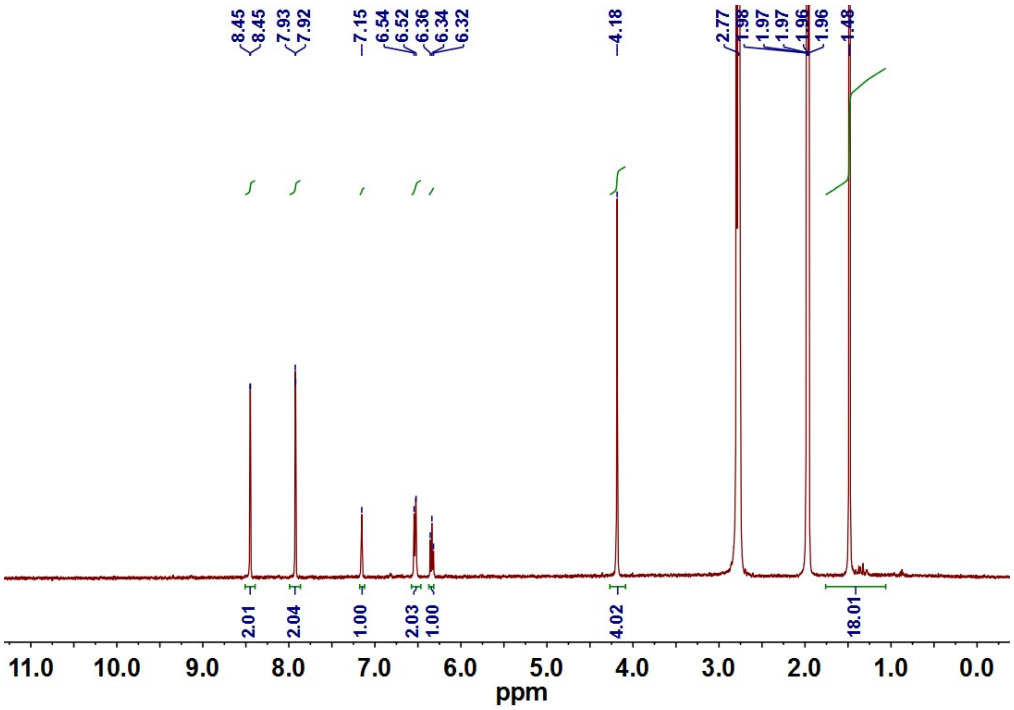

Figure S42. ^{1}H NMR spectrum of macrocycle **1** in CD_3CN (D_2O exchange) at 298 K.

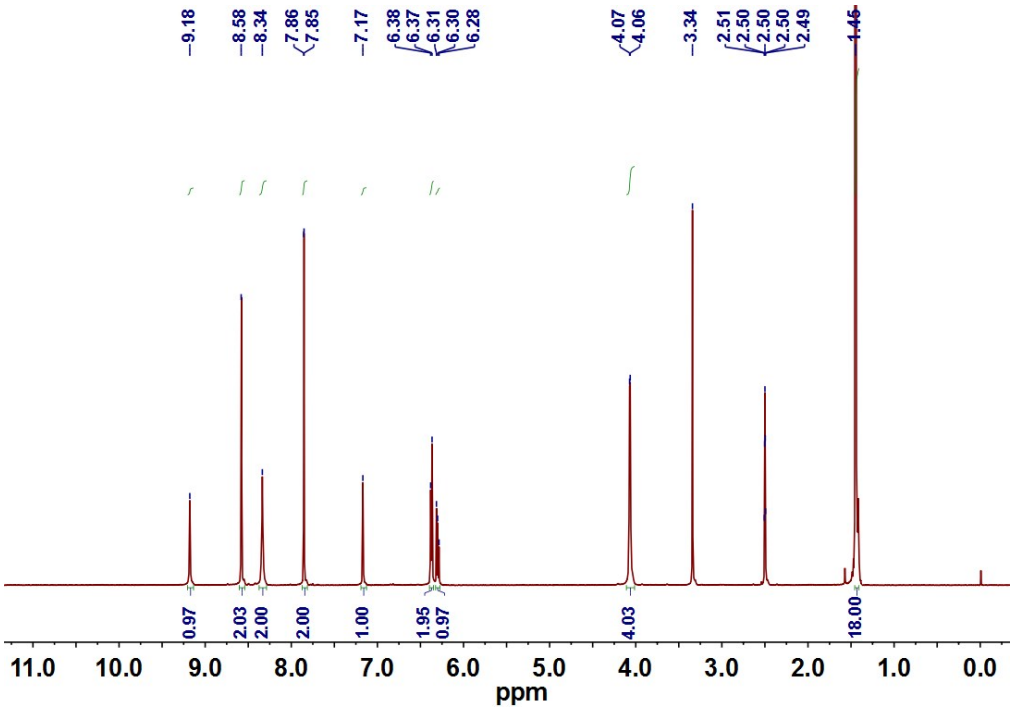

Figure S43. ^{1}H NMR spectrum of macrocycle **1** in DMSO-d_6 at 298 K.

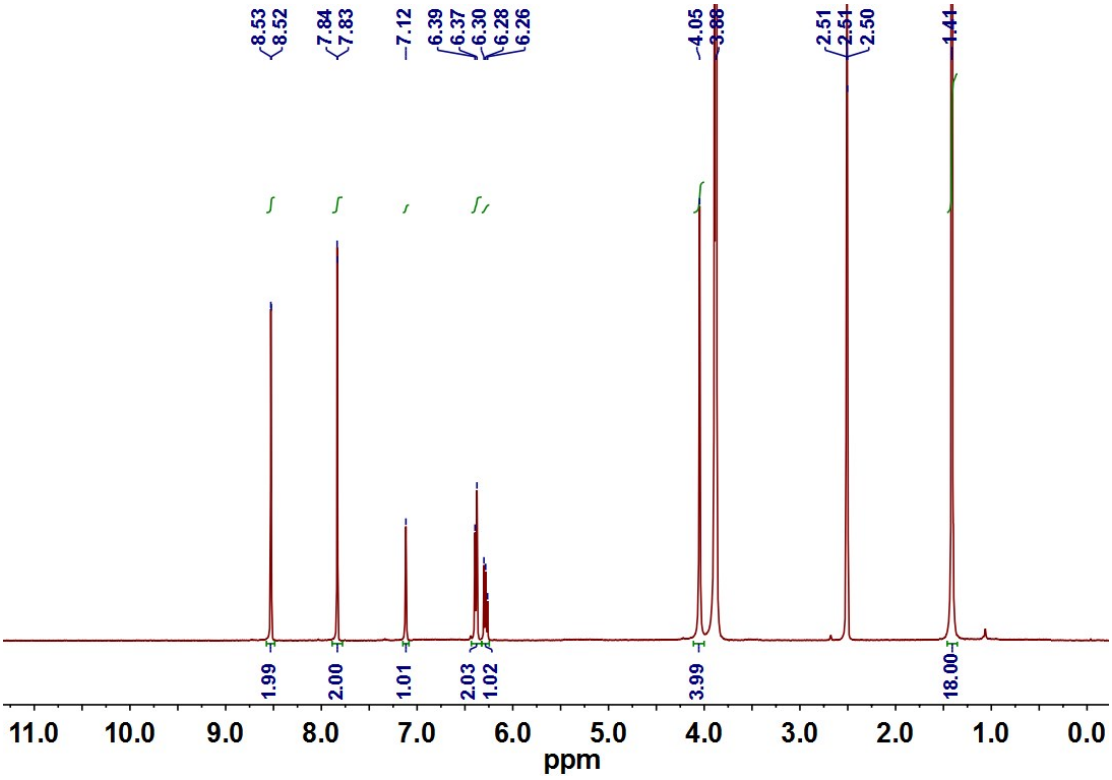

Figure S44. ^{1}H NMR spectrum of macrocycle **1** in DMSO-d_6 (D_2O exchange) at 298 K.

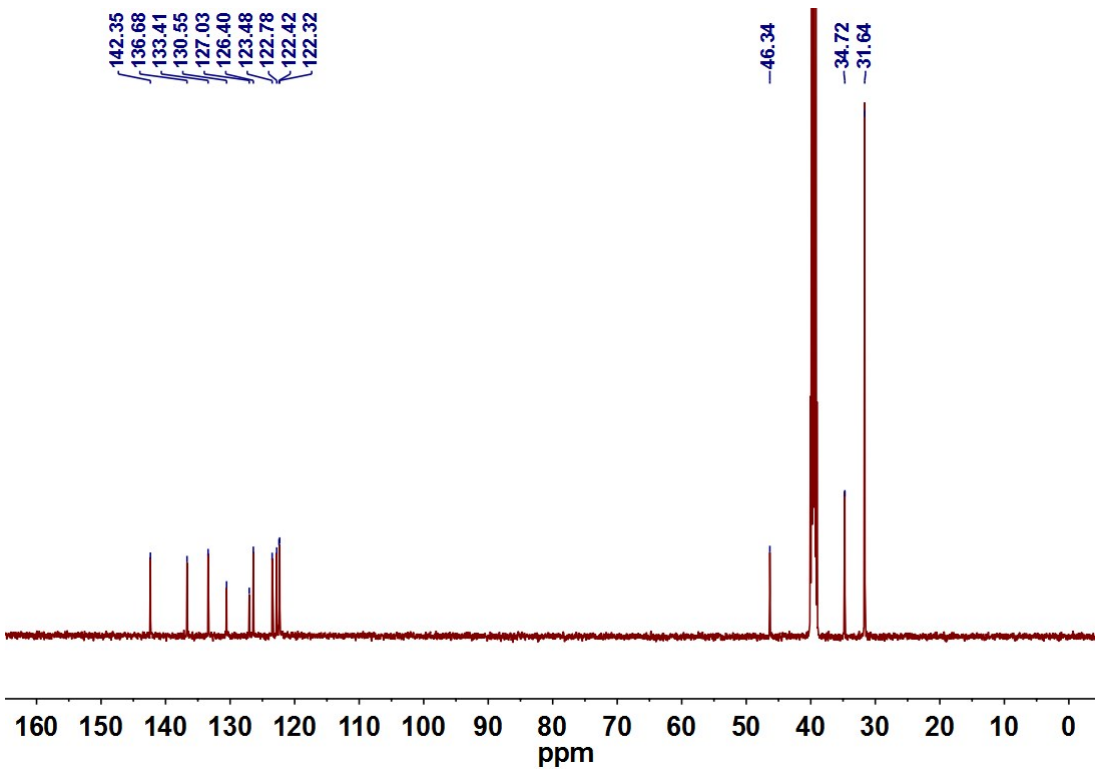

Figure S45. ^{13}C NMR spectrum of macrocycle **1** in DMSO-d_6 at 298 K.

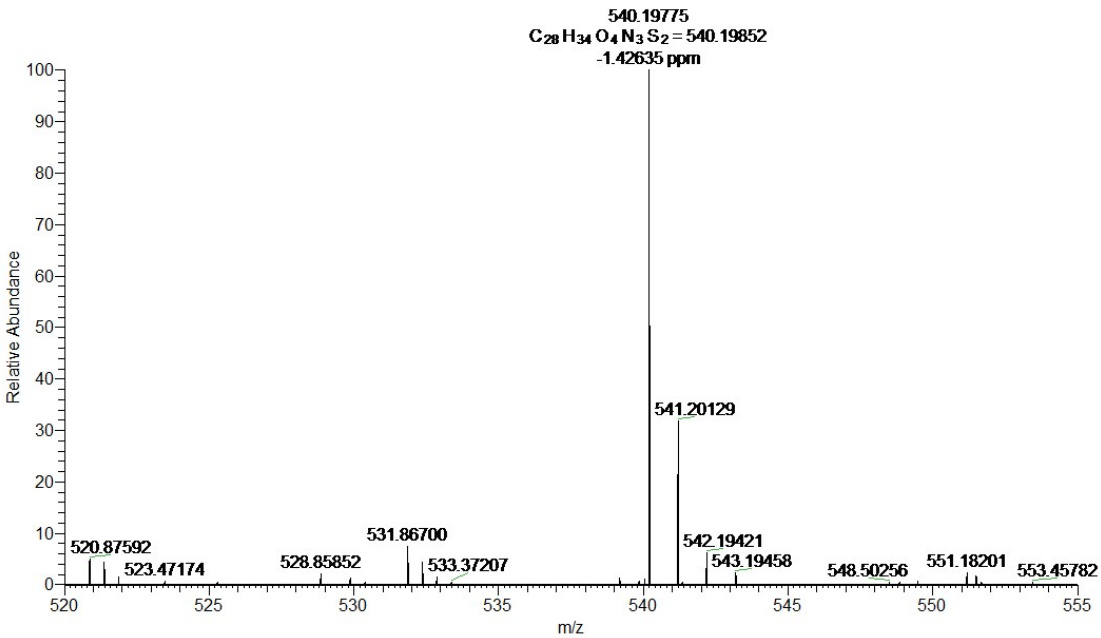

Figure S46. HRMS-ESI spectrum of macrocycle **1**.

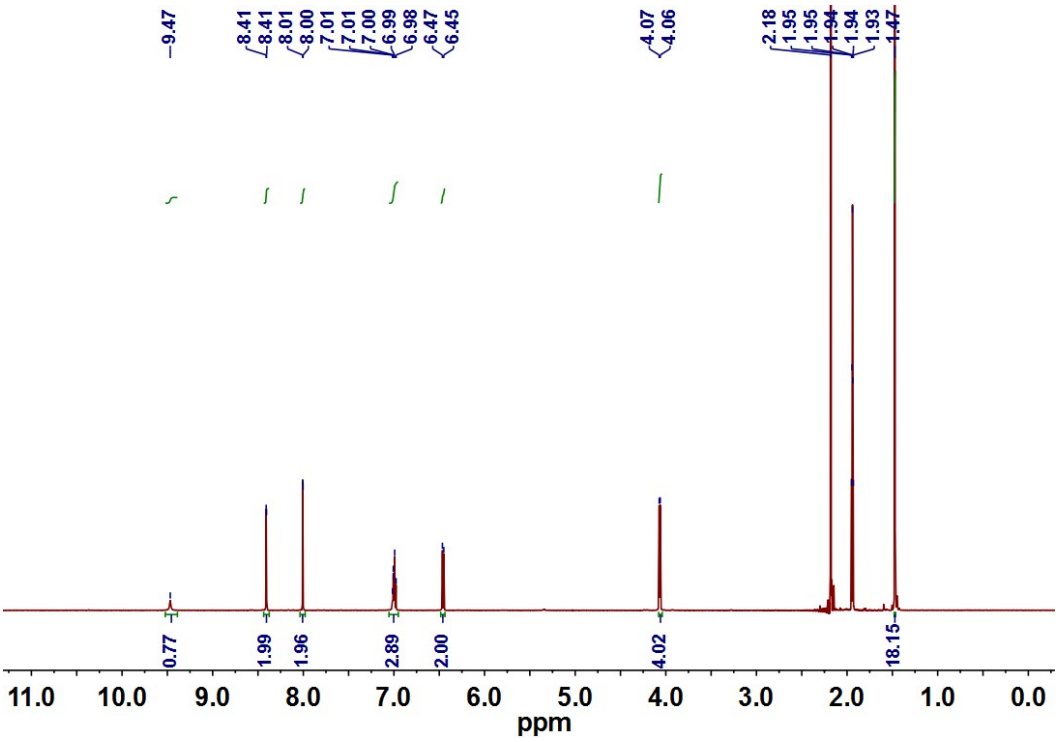

Figure S47. ^{1}H NMR spectrum of macrocycle **2** in CD_3CN at 298 K.

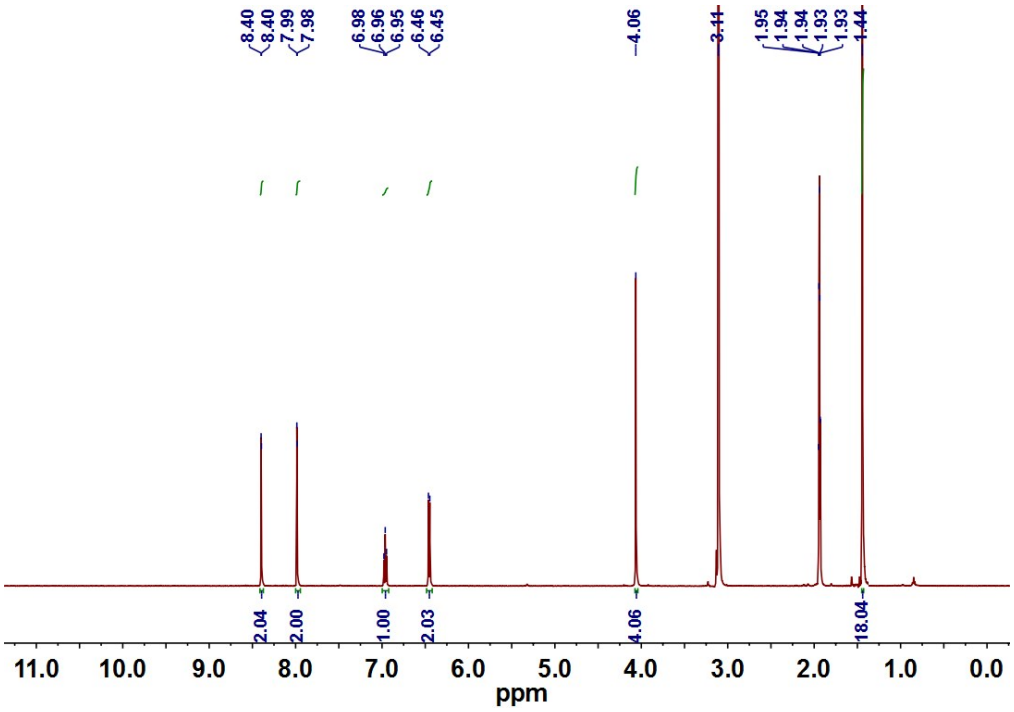

Figure S48. ^{1}H NMR spectrum of macrocycle **2** in CD_3CN (D_2O exchange) at 298 K.

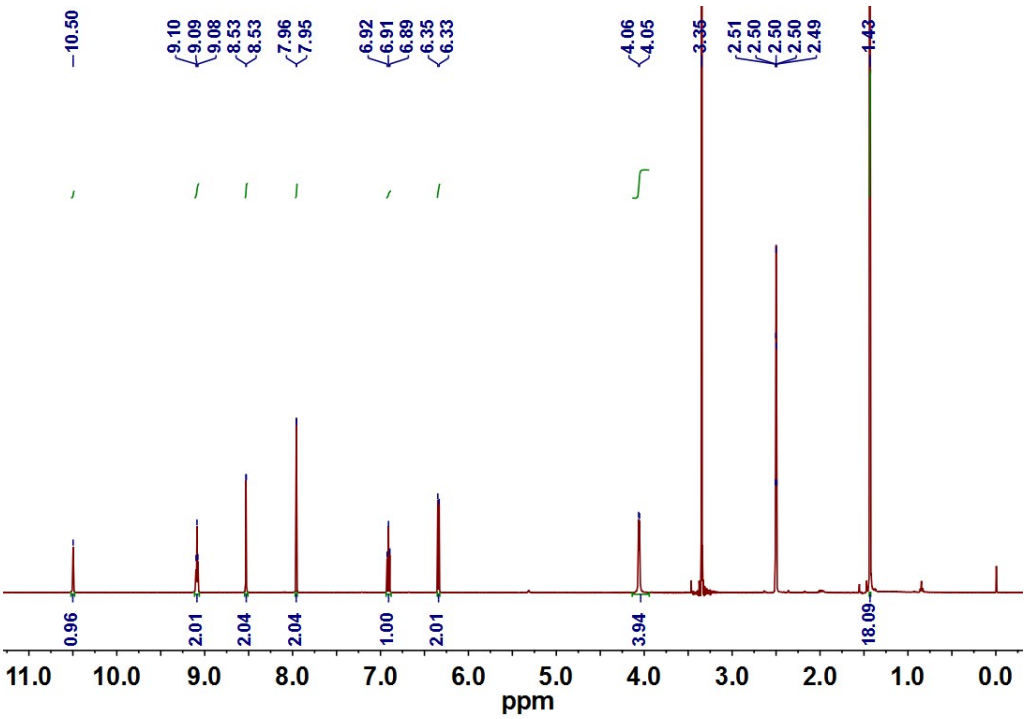

Figure S49. ^{1}H NMR spectrum of macrocycle **2** in DMSO-d_6 at 298 K.

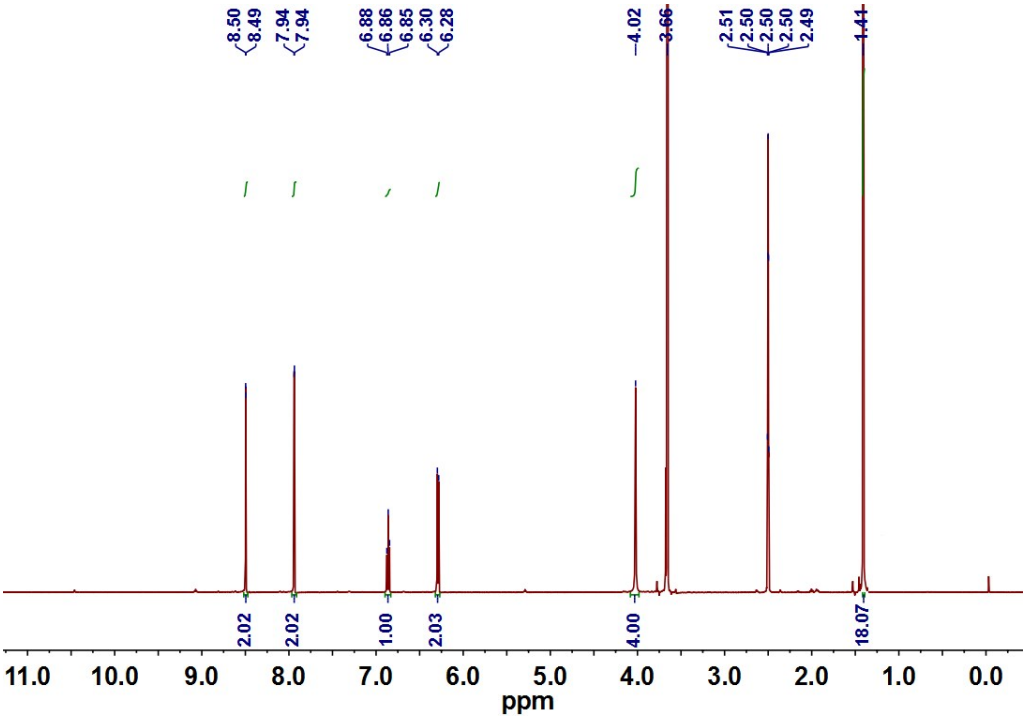

Figure S50. ^{1}H NMR spectrum of compound **2** in DMSO-d_6 (D_2O exchange) at 298 K.

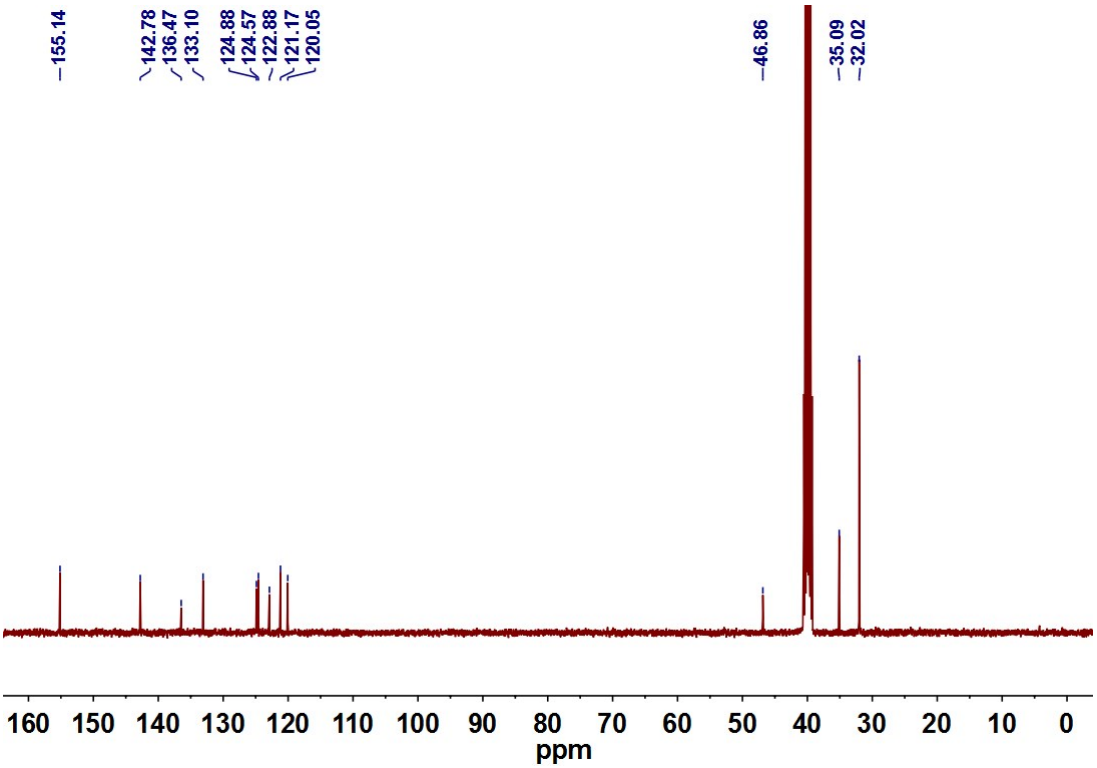

Figure S51. ^{13}C NMR spectrum of macrocycle **2** in DMSO-d_6 at 298 K.

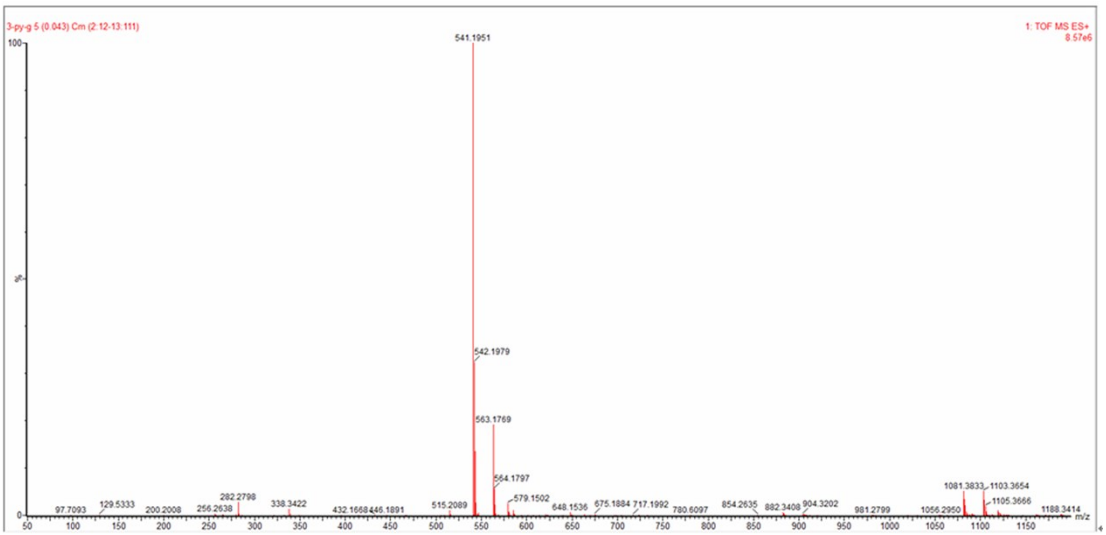

Figure S52. HRMS-ESI spectrum of macrocycle **2**.